Geochemical features and relative B-Li-Cl compositions of deep-origin fluids trapped in high-pressure metamorphic rocks

Kenta Yoshida[a*], Takao Hirajima[a], Shinji Ohsawa[b], Tomoyuki Kobayashi[a,b,c], Taketoshi Mishima[b] and Yoshiteru Sengen[a]

[a] *Department of Geology and Mineralogy, Graduate School of Science, Kyoto University, Kitashirakawa Oiwakecho, Kyoto 606-8502, Japan*

[b] *Beppu Geothermal Research Laboratory, Institute for Geothermal Sciences, Graduate School of Science, Kyoto University, Noguchibaru, Beppu 874-0903, Japan*

[c] *Faculty of Health & Sports Sciences, Nagoya Gakuin University, Seto Kamishinano-cho, Aichi 480-1298, Japan*

ABSTRACT

The relationships between the relative B-Li-Cl compositions of deep fluids and their entrapment depth were investigated by means of geochemical studies of fluid inclusions in foliation-parallel quartz veins using the crush-leach method and conventional petrology. Investigated samples were collected from the Sanbagawa metamorphic belt, SW Japan, covering the metamorphic grade from the pumpellyite-actinolite facies (300 ºC/ 0.5 GPa) to the quartz-eclogite facies (550-650 ºC/ 1.5-2.5 GPa). We took a special care on the relationship between arrangements of fluid inclusions and grain fabric of their host quartz to evaluate the entrapment timing of fluid inclusions. Our results show that quartz veins can be classified into three groups based on their fabrics: polygonal type (P-type), deformed-interlobate-grain type (DI-type) and pervasively-deformed-domain type (DD-type). P-type fabrics in the studied samples indicate textural development under the conditions of very low differential stress with relatively high temperature and free from subsequent brittle deformation, thus, the corresponding fluid inclusions should have been trapped during the peak metamorphic stage or in the early stage of exhumation. On the other hand, fabrics of DI- and DD-type, such as largely

deformed lamellae and undulatory extinction, are thought to be formed under high differential stress and low temperatures (<400 ºC) during the later stage of exhumation. Fluid inclusions in DI-/DD-type veins are thought to be trapped in association with the later-stage deformation event and corresponding fluid infiltration. P-type veins tend to contain relatively high saline aqueous fluids (5-10 mass%$_{NaCleq}$) and their compositions are mainly Na-Cl dominated. DI-/DD-type veins contain dilute aqueous fluid (<5 mass%$_{NaCleq}$) and some of them are characterized by the dominance of HCO_3 in anions. The relative B-Li-Cl compositions of the studied fluids are characterized by high (B+Li)/Cl ratio, which is characteristics of the Arima-type hydrothermal fluids, thought to be directly derived from the subducting-slab at the present fore-arc region of the Japanese island chain. The Li/B ratios of the studied fluids show a large variation from a low value of 0.02 in the pumpellyite-actinolite facies/ DD-type sample to a high value of 1.99 in the eclogite facies/ P-type sample. These results suggest that high-saline and B-Li-enriched fluids are supplied from subducting slabs to the hanging wall mantle wedge in the subduction zone.

Keywords: Fluid inclusions; aqueous fluid; B-Li-Cl composition; crush-leach method; Sanbagawa metamorphic belt

*Corresponding author at: Department of Geology and Mineralogy, Graduate School of Science, Kyoto University, Kitashirakawa Oiwakecho, Kyoto 606-8502, Japan. Tel.: +81 75 7534150; E-mail address: yoshikem@kueps.kyoto-u.ac.jp (K. Yoshida).

1. Introduction

Aqueous fluids in subduction zones play an important role in geochemical and geophysical processes, such as slab seismicity, arc magmatism, metamorphism, mantle metasomatism, and the

transport of several components from the surface to deep parts of the Earth (Tatsumi, 1989; Bebout, 2007; Hacker, 2008). Such fluids are generally believed to originate from mineral-bound water in hydrous minerals in the subducting materials, and pore-fluids carried by oceanic sediments. The latter are occasionally assumed to be expelled at very shallow depths (<~5 km) due to compaction (Peacock, 1990; Jarrard, 2003; Hacker, 2008); however, some amount of marine pore-fluids survive at depths of ~100 km (Sumino et al., 2010). Although dehydrated aqueous fluids have been treated as pure water as a first approximation in many previous studies, natural aqueous fluids found from metamorphic rocks are actually aqueous solutions that contain several solutes, sometimes showing higher salinity than halite saturation (Yardley & Graham, 2002). The solute of the aqueous fluids, such as the chlorine content, significantly increases the solubility/mobility of crustal components such as silicate minerals and also REE(rare earth elements)-bearing minerals (e.g., Newton and Manning, 2010; Higashino et al., 2013), thus the chemical compositions of major elements in natural deep fluids provide indispensable information for understanding the role of deep fluids in subduction zones.

Minor light elements such as Li, B and Be are thought to be good tracers during fluid migration and fluid-rock interaction including hydrothermal alteration in oceanic crusts and dehydration/hydration reactions in subduction zones (Bebout, 2007; Bebout et al., 1999; Konrad-Schmolke et al., 2011; Marschall et al., 2009; Seyfried et al., 1984). Those elements tend to be relatively highly concentrated in altered oceanic crusts and pelagic sediments (Donnelly et al., 1980; Shaw et al., 1977; Leeman & Sisson, 1996) because of the high temperature hydrothermal process (Seyfried et al., 1984). To quantify the mass transport during the subduction zone processes, behaviors of Li, B and Be in hydrothermal systems have been investigated experimentally (You et al., 1996; Kogiso et al., 1997; Brenan et al., 1998; Tenthorey & Hermann, 2004; Kessel et al., 2005). Experimental and natural sample studies have determined preliminary estimates of partition coefficients of these elements (Brenan et al., 1998; Tenthorey & Hermann, 2004; Marschall et al.,

2006). Based on simple mass balance calculations, some studies indicated that the concentration ratios of the above-mentioned elements in fluid, i.e. Be/B, B/Cl, and Li/B, increase with dehydration degree, that is to say, the development of metamorphism (Bebout et al., 1993; Scambelluri et al., 2004; Marschall et al., 2007). It should be noted that such mass balance calculations are strongly depending on the whole rock compositions and related whole rock partition coefficients (Domanik et al., 1993; Marschall et al., 2007; Yoshida et al., 2011).

Recent geochemical studies of hot- and mineral-springs indicate that B- and/or Li-rich hot-spring waters are directly derived from the subducting-slab to the surface region upward to the crustal surface (Ohsawa, 2004; Ohsawa et al., 2010; Kazahaya et al., 2014). Ohsawa (2004) and Kazahaya et al. (2014) suggested that the high Li/Cl ratio of hot-spring water is an indicator of the deep-origin slab derived fluid, so called Arima-type hydrothermal fluids (Matsubaya et al., 1973). Such fluids are characterized by high salinity, δ^{18}O value, and ^{3}He/^{4}He ratio with low δD compared to the modern sea water. Ohsawa et al. (2010) also pointed out that the composition of hot-spring waters collected from the Miyazaki plain, in the fore-arc region of southwest Japan, are high in B concentrations, and that their high B/Cl ratio are originated from the diagenetic dehydration of smectite at around 130^{o}C. They showed that some Li- and B-rich spring waters originated from diagenetic/metamorphic processes and also experienced subsequent groundwater dilution.

Fluid inclusions preserved in H*P*/L*T* metamorphic rocks provide direct information on the subduction-related fluids which develop under the fore-arc to sub-arc region, and provide clues to interpret the results of the geochemical studies mentioned above. However, few studies deal with the trace element chemistry of the fluid phase, because of the difficulty of the analysis mainly derived from the small size of fluid inclusions, even though a number of fluid inclusion studies have been performed with respect to the metamorphic and/or tectonic processes (Boullier, 1999; Küster & Stöckhert, 1997; Bakker & Mamtani, 2000; Touret, 2001; Van den Kerkhof, 2001; Krenn et al., 2008; Nishimura et al., 2008; Krenn, 2010). One possible solution to this problem is the crush-leach

method (Bottrell et al., 1988; Banks & Yardley, 1992) applied to quartz veins developed in parallel with the main foliation of the metamorphic rocks, which are capable of retaining pre-peak-/peak-metamorphic stage fluids as fluid inclusions (Nishimura et al., 2008; Yoshida & Hirajima, 2012).

In order to directly determine the chemical compositions of deep fluids and evaluate their signature with respect to their entrapment depth, we carried out systematic sampling of foliation-parallel quartz veins in the Sanbagawa belt, Japan, which covers the formation depths from ca. 15 km to 60 km, and performed petrographical and geochemical studies on fluid inclusions. Our results show that fluid inclusions in such quartz veins have highly Li- and B-enriched compositions similar to those of Arima-type hydrothermal fluids. In addition, among the studied samples, quartz veins with less-deformed textures retain fluid inclusions with higher salinities, though still high Li/Cl and/or B/Cl compositions. In this paper, we show the mode of occurrence and chemical characteristics of fluid inclusions trapped in quartz veins. We also discuss the relative B-Li-Cl compositions of the fluids and their significance to geofluid evolution during prograde metamorphism in subduction zones. Mineral abbreviations used in this paper are after Whitney and Evans (2010).

2. Analytical method

2.1. Mineral chemistry

Chemical compositions of minerals were analyzed with an electron microprobe analyzer with five wavelength-dispersive spectrometers (JEOL, JXA-8105) at the Department of Geology and Mineralogy, Kyoto University. Some qualitative and semi-quantitative analyses were also performed on a scanning electron microprobe (HITACHI, S-3500H) equipped with an energy-dispersive spectrometer (EDAX, Phoenix) at Kyoto University.

2.2. Microthermometry

Microthermometric measurements of fluid inclusions were performed using a heating and cooling stage (LINKAM, LK-600) at the Department of Geology and Mineralogy, Kyoto University. The stage was calibrated with a melting-point of synthetic fluid inclusion standards (10 mass% NaCl solution and pure water). The accuracy of the ice melting temperatures within the range -80 to 0 ºC was estimated to be ±0.1 ºC at a heating rate of 2 ºC/min, and for the homogeneous temperatures within the range from 0 to 400 ºC, was ± 1 ºC at a heating rate of 10 ºC/min. Melting temperatures of aqueous fluids were converted into Na-Cl equivalent salinity ($mass\%_{NaCleq}$) using the equation of Bodnar (1993).

2.3. Fluid inclusion chemistry

The qualitative analysis of fluid inclusions was carried out by using a laser RAMAN spectrophotometer (JASCO, NRS-3100) at the Department of Geology and Mineralogy, Kyoto University using the 514.5 nm line of Ar-ion at 10-80 mW with a spot size of 1.0 μm on the surface. Calibration was performed using a 520 cm^{-1} Si-wafer band and neon spectrum.

To determine the chemical characteristics of the aqueous fluid of fluid inclusions, we extracted fluids using the crush-leach method after Bottrell et al. (1988) and Banks and Yardley (1992). To prepare pure quartz grains, the vein sample was roughly crushed and sieved into 425–2000 μm size. Quartz grains without extraneous matters were handpicked under a stereoscopic microscope. Separated quartz grains were boiled in concentrated nitric acid and rinsed with ultrapure water to eliminate impurities. Some 50 g of cleaned sample was milled into white powder in an agate mortar, in order to crush-out the fluid inclusions. The milled powder was, then, transferred to a Teflon bottle and a solute of fluid inclusions were leached with 50–60 mL of ultrapure water (Wako Pure Chemical Industries, Ltd.: solutes are less than 10 pg/g in each element) as a “fluid inclusion solution” for major/trace component analysis. The solution sample with quartz powder was filtered out with 0.22 μm mesh filter before chemical analysis. Na^+, K^+, Ca^{2+}, Mg^{2+}, NH_4^+, F^-, Cl^- and SO_4^{2-}

were analyzed by an ion chromatography (DIONEX, DX-120) at the Institute for Geothermal Sciences, Kyoto University, Beppu, Japan. The bicarbonate ion content was calculated by the valance of charge. Li and B were analyzed by ICP-MS at TOSOH Analysis and Research Center, Nan-yo City, Yamaguchi, Japan. Blank values for the crush-leach technique were obtained either by water soaked in a Teflon bottle for about 12 hours to evaluate the contamination from the Teflon bottles (blank1), by rubbing the agate mortar and pouring ultrapure water into the mortar to be treated in the same manner as the samples for the contamination from the air and mortar (blank2). The values obtained from the blank1 is near zero and negligible, while blank2 contained a low amount of Li (0.11 μg/L) and a considerable amount of B (9.5 μg/L), which were subtracted from the raw data of the sample concentrations.

3. Geological background

Studied samples were collected from the Sanbagawa metamorphic belt, which is exposed in southwest Japan (Fig. 1a). The Sanbagawa metamorphic belt is divided into four mineral zones based on the mineral assemblages of pelitic schists (Kurata & Banno, 1974; Enami, 1982; Higashino, 1990): chlorite, garnet, albite-biotite and oligoclase-biotite zones. Peak metamorphic *P-T* conditions of the four mineral zones were estimated as 300 ºC/ 0.5 GPa for the lowest grade chlorite zone which is pumpellyite-actinolite facies equivalent, through 440–480 ºC/ 0.7–0.85 GPa for the garnet zone and 520–540 ºC/ 0.8–0.95 GPa for the albite-biotite zone, to 610 ºC/ 1.0 GPa for the highest grade of oligoclase-biotite zone which is epidote-amphibolite facies equivalent (Enami, 1994). In central and eastern Shikoku, eclogite facies rocks are also locally present (Takasu, 1984; Wallis & Aoya, 2000; Ota et al., 2004). These eclogitic rocks show a pressure gap against the surrounding non-eclogitic rocks, and some of them show different metamorphic histories before the juxtaposition with above-mentioned non-eclogitic rocks of the Sanbagawa belt (Takasu, 1984; Kunugiza et al., 1986).

Specifically, the investigated samples were collected from the Besshi area in central Shikoku (Fig. 1b) and the Wakayama area on Honshu Island (Fig. 1e). In the Besshi area, two eclogite units, the Western Iratsu (WI) body and the Seba (SB) body, and their neighboring non-eclogitic areas (Fig. 1c/d) were investigated. The WI body is thought to have undergone two distinct stages of subduction-related metamorphism, referred as M1 and M2, whose peak metamorphic conditions were estimated as ca. 660 ºC/ 1.2 GPa and 550–680 ºC/ 1.4–2.0 GPa, respectively (Fig. 1f: Endo, 2010; Endo et al., 2012). Peak metamorphic conditions of the Seba body are estimated as 520–640 ºC/ 1.3–2.4 GPa (Aoya, 2001; Zaw et al., 2005). Recent studies found remnants of eclogite facies metamorphism around these eclogite bodies by Raman microscopy and indicated the areal extension of the eclogite facies metamorphism (e.g., Kouketsu et al., 2010; 2014). As a result, these eclogite bodies are considered to have consisted in a continuous eclogite-nappe at eclogite facies conditions and have been juxtaposed with non-eclogitic rocks together (Fig. 1c: Aoya et al., 2013; Wallis and Aoya, 2000). The surrounding part of these eclogite units mainly belong to the albite- and oligoclase-biotite zone of the Sanbagawa metamorphic belt. Samples of lower metamorphic grades were collected from the Wakayama area where the chlorite, garnet and biotite zones are exposed (Fig. 1e: Makimoto et al., 2004). Since oligoclase is not observed in the biotite zone, the biotite zone of the Wakayama area is thought to be equivalent to the albite-biotite zone of central Shikoku. Thus, the samples investigated in this study cover the peak pressure range of 0.5–2.5 GPa and the temperature range of 300–610 ºC (Fig.1f).

4. Investigated samples

In order to determine the deep fluid characteristics, we studied quartz veins developed parallel with the main schistosity of the host rocks (hereafter foliation-parallel quartz vein) (Fig. 2a-c). Some veins show the boudinaged shape concordant with the deformation structure of the host metamorphic rock indicating pre-tectonic existence of veins (Fig. 2a, c), whereas others display a foliation-parallel

occurrence concordant with the less deformed structure of the host rock (Fig. 2b). Such kind of veins has a potential to retain the fluid trapped during prograde or near-peak metamorphic stages (Nishimura et al., 2008; Yoshida and Hirajima, 2012). The studied veins are almost monomineralic, except for some samples containing very small amount of accessory minerals such as rutile and phengite. Six samples from the non-eclogitic area and five samples from the eclogite unit were investigated in this study. A quartz vein sample crosscutting the main schistosity of the host rock was also investigated to reveal the character of fluid activity during the very later stage of exhumation of the Sanbagawa belt (Fig. 2d). In this section, we describe the characteristics of the host rocks.

Volume fractions of the main constituent minerals of the host metamorphic rocks were determined using X-ray mapping of major elements for nine samples (Table 1). For the other two samples, simple point counting based on either semi-quantitative multi-point analysis using EDX (Matsumoto & Hirajima, 2006) or optical microscopic observation was performed. Among the investigated samples, no boro-minerals or possible lithia-mineral were observed. Representative chemical compositions of mica, amphibole, and apatite which are candidate for the container of the halogens at peak metamorphic conditions, are shown in the supplementary material (Table S1-S3). However, all mica and amphibole contain no or scarce amount of halogens (mostly <0.01 wt%) and there is no obvious relationship between halogen content of minerals and fluid inclusion composition described in the following section. Apatites observed in some samples also contain small amount of Cl (up to 0.2 wt%) and are classified as fluorapatite (Table S3).

1. Chlorite zone (mafic: WS04)

One mafic rock sample (WS04) was chosen as a representative sample for the chlorite zone. WS04 is composed of the main metamorphic minerals: epidote, chlorite, actinolite, phengite, albite, titanite and quartz with a small amount of chalcopyrite. Later stage calcite veins cutting the main schistosity are locally developed.

2. Garnet zone (mafic: WS02)

The investigated mafic schist (WS02) mainly consists of epidote, chlorite, amphibole, albite and phengite with small amounts of calcite, titanite and apatite. Later-stage calcite veins are also observed. Albite porphyroblasts contain epidote, chlorite, amphibole, quartz, calcite and titanite. Compositions of amphibole are from actinolite to magnesiohornblende.

3. Albite-biotite zone (mafic: 07113002)

This sample mainly consists of albite, phengite, epidote, amphibole, titanite and calcite with accessory apatite and chalcopyrite. Compositions of the amphiboles are barroisite and magnesiohornblende.

4. Albite-biotite zone (pelitic: SD09, IR28)

These samples are mainly composed of quartz, phengite, chlorite, albite and garnet with additional phases such as apatite (SD09) and amphibole (IR28). The garnet shows Mn bell shape type zoning with X_{Sps} up to 0.31 at their apparent core. SD09 was collected near the boundary between the suggested eclogite-nappe and the surrounding lower grade part, however, no remnant of eclogite-facies metamorphism was found in the SD09 sample, thus this sample is treated as a non-eclogitic sample.

5. Oligoclase-biotite zone (pelitic: IR27)

IR27 is a metapelite composed of quartz, phengite, plagioclase, garnet, amphibole and epidote with small amounts of iron oxide and rutile. Plagioclase contains anorthite component up to 10 mol%. The garnet shows Mn bell shape type zoning with X_{Sps} up to 0.26 at their apparent core.

6. Eclogite unit (mafic: SSB03, SSB04, SEBA, SSB19)

Four mafic rocks were collected from the Seba eclogite body. They consist mainly of quartz, phengite, garnet, chlorite, amphibole, epidote, rutile and hematite. SEBA and SSB19 contain clinopyroxene (omphacite). In addition, SEBA contains biotite frequently associated with garnet, which was probably a product of the decompression stage. SSB03 and SSB04 are free of clinopyroxene even though they are collected from the eclogite unit, probably because of the bulk rock composition. SEBA and SSB19 underwent rehydration reactions that decomposed clinopyroxene to symplectite with varying degrees, which is mainly composed of amphiboles and plagioclases.

7. Eclogite unit (metasediment: IR04)

The protolith of IR04 is thought to be a sedimentary rock with unique composition with very low SiO_2 content and contain very high amount of amphibole and phengite (>40 vol% respectively) (Yoshida & Hirajima, 2012). The main constituent minerals are amphibole, phengite and garnet with small amounts of retrograde chlorite and albite. Accessory rutile, apatite and quartz are also observed.

8. Later stage vein (10AS18)

Sample 10AS18 was collected from the chlorite zone of the Asemigawa area, central Shikoku (Fig. 1b). The vein of 10AS18 crosscuts the foliation of the host rock, indicating that it was formed at the later stage of exhumation after the peak *P-T* conditions of the chlorite zone. Therefore, sample 10AS18 is thought to contain fluids trapped at the lowest metamorphic conditions (<300 ^{o}C and <0.5 GPa) during the retrograde evolution.

5. Macro and microscale structure of quartz veins

Macroscale observations show that foliation-parallel quartz veins collected from the WI body and its proximal area (IR04, IR27 and IR28) are almost free from obvious deformation structure (Fig. 2b). On the other hand, quartz veins collected from the Seba eclogite body and the Wakayama area experienced deformation resulting in a boudinaged shape of several degrees (Fig. 2a/c). However, some of the boudinaged samples have less-deformed microstructure, as described below.

The studied foliation-parallel quartz veins are classified into two groups based on the quartz grain fabrics: one is less-deformed polygonal fabric type (P-type, Fig. 3a/b) and the other is pervasively deformed and recrystallized type (Fig. 3c/d). The latter type veins are further subdivided into two groups on the basis of their grain size: interlobate fabric type (DI-type, Fig. 3c) with relatively smaller grains (<~1mm) and pervasively deformed domain type (DD-type, Fig. 3d). No quartz grains showed fibrous textures among the studied samples.

Six samples collected from the eclogite bodies and their proximal area (SSB03, SSB04, SEBA, IR04, IR27 and IR28) are classified as P-type (Fig. 3a, b, Table 2). These veins are characterized by polygonal fabric with coarse grains up to 5 mm in diameter, which is identical to the “foam microstructure.” This type of texture is thought to be formed under relatively high temperatures (>300–400^{o}C) and low differential stress in the deep crust (Stöckhert et al., 1997; Krenn, 2010; Passchier & Trouw, 2005). Fluid inclusions in P-type veins are arranged along specific planes developed in intragranular and/or transgranular settings.

SSB19 and SD09 are DI-type, which is characterized by interlobate fabrics with grains of various sizes. Most samples of this type show seriate grain size distribution with the largest grain size of ca. 2 mm. Coarse grains in DI-type veins sometimes show deformation lamellae and/or undulatory extinction (Fig. 3c), suggesting that they underwent tectonic stress and deformation at low-grade metamorphic conditions (300–400 ºC). DI-type veins contain fluid inclusion comprising specific

planes or dusty clusters.

Samples collected from the non-eclogitic area in the Wakayama area (07113002, WS02, and WS04) and the foliation-cutting vein sample 10AS18 collected from the chlorite zone of the Asemigawa area are classified as DD-type. Most part of DD-type veins shows no obvious grain boundaries (Fig. 3d) and there appear the pervasive deformed domains, the sizes of which are sometimes larger than several centimeters. Most fluid inclusions in DD-type veins occur in randomly-oriented transgranular plane developed at subgrain boundaries.

6. Characteristics of fluid inclusions

6.1. Microtexture, microthermometry and chemical species

Within the studied quartz veins, single or multiple fluid inclusion groups (FIAs) are observed in each sample. Microthermometric data and textural characteristics are shown in Table 2. All the observed fluid inclusions were arranged along intragranular (Fig. 4a) or transgranular planes (Fig. 4b) except for one sample (SSB03c) containing isolated type. Among the observed FIAs, four fluid inclusion types are identified based on their chemical species and salinity of aqueous fluid: type 1) diluted aqueous fluids near to or lower than sea-water salinity (<3–5 mass% $_{NaCleq}$); type 2) relatively high saline aqueous fluids (>5 mass%$_{NaCleq}$); type 3) high saline fluids exceeding halite saturation; type 4) anhydrous fluids. The ice melting temperature (T_m) as well as the total homogenization temperature (T_h) were measured for the aqueous fluid inclusions. All measured fluid inclusions homogenized into one phase below 350 ºC. Average values and ranges of T_m and T_h are shown in Table 2 and histograms of the microthermometric data are available as supplementary data (Fig. S1).

Type 1 fluid inclusions accompany with or without some volatile gaseous component such as N_2 or CH_4. Type 1 is further divided into the following classes: type 1A arranged along intragranular planes, type 1B arranged along transgranular planes and type 1C scattered along subgrain boundaries

(a kind of transgranular plane, distinct from ordinary ones). However, microthermometry results of these subtypes are very similar. Average T_m of type 1 inclusions are concentrated between -0.2 to -2.0 ºC and average T_h are between 170 to 241 ºC, except for later-stage fluid (10AS18: T_h = 137).

Type 2 fluid inclusions are arranged along intragranular (type 2A) or transgranular planes (type 2B). Average T_m of type 2 fluid inclusions in four fluid inclusion groups vary from -4.9 to -8.6 ºC, obviously lower (i.e., higher in salinity) than the modern sea water. Average T_h for each sample also show a range from 202 to 250 ºC (Table 2). Type 2 fluid in SSB03 (SSB03a) has a relatively wide range of T_m (-3.0 to -18 ºC), although the systematic relationship between salinity, volatile compositions, and occurrences are hardly recognized.

Type 3 fluid inclusions are very rare, recognized only in SSB03 (SSB03c) and shows isolated occurrence with very high salinity, exceeding halite saturation (Fig. 4g).

Fluid inclusions of type 4 are characterized by dark color with one or two phases without H_2O (Fig. 4d). They are also subdivided into intragranular type 4A and transgranular type 4B. All fluid inclusions of type 4 contain N_2 and CH_4 except for SSB03b, which contains only N_2. SD09a and SSB04c contain CO_2 in addition to N_2 and CH_4 and IR04c has the further addition of H_2.

Estimation of the total volume of fluid inclusions contained in a specific volume of bulk sample is difficult, since they occur as discrete assemblages along healed cracks. Therefore it is difficult to denote quantitatively which fluid inclusion group is most dominant in the sample containing multiple fluid inclusion groups, and thus, the abundances of each fluid inclusion group are roughly presented in Table 2.

6.2. Hydrochemical facies of crush-leached fluids

The chemical compositions of the crush-leached fluids are shown in Table 3. Note that these data do not represent absolute concentration of each element of the fluid inclusions, but the result of diluted "fluid inclusion solutions" obtained by the crush-leach method. The ratio of the major components,

i.e. Na^+, K^+, Ca^{2+}, Mg^{2+}, Cl^-, HCO_3^{2-} and SO_4^{2-} of the crush-leached fluid are shown in a “Piper’s diagram” (Fig. 5, constructed after Piper, 1944). Hydrochemical characteristics are considered based on the most concentrated components among anions and cations. The studied crush-leached fluids are divided into three types: Na-Cl type, X-HCO_3 type (X refers to Na or K) and intermediate type. Most fluid samples have either Cl or HCO_3 as the major anion and are mostly free of F or SO_4. All Cl-dominated samples contain Na as the primary cation. On the other hand, HCO_3 dominated samples contain Na or K as primary cations. Two samples, 07113002 and WS02, contain considerable amounts of both Cl and HCO_3, and are classified as intermediate type. The threshold to be included in the intermediate type is defined as $0.67 < Cl/HCO_3 < 1.5$ (in mass ratio).

As shown in Fig. 5, samples SSB04, SSB03, SEBA, IR04 and IR27 are classified as Na-Cl type, and samples IR28, SSB19, SD09, WS04 and the later stage vein of 10AS18 are as X-HCO_3 type. Two mafic-hosted samples, 07113002 and WS02, are intermediate type.

6.3. Relative B-Li-Cl composition of crush-leached fluids

Li, B and Cl characteristics of the crush-leached fluids are shown in the B×500-Li×2000-Cl ternary diagram after Ohsawa et al. (2010), concerning with the hydrochemical characteristics and lithotype of the vein-hosting–rock (host rock) (Fig. 6). Quartz vein samples hosted by sedimentary and mafic rocks are shown in Fig. 6a and 6b, respectively. Shape of marks and filled colors show hydrochemical characteristics of major components and metamorphic grade of host rocks, respectively.

Na-Cl type fluid extracted from metasediment-hosted veins (IR27 and IR04) have a high (B+Li)/Cl ratio and are plotted near the B-Li side of the ternary diagram (Fig. 6a), although some of them show higher salinity than modern seawater and have a high Cl content (cf. Table 2). Their Li/B ratios are very high (1.70 and 1.99, respectively) compared to other samples, meaning those samples are rich in both Li and B. Na-Cl type samples extracted from mafic-rock-hosted veins were all

collected from the Seba eclogite body. The Li/B ratios of these samples show a range of 0.10–0.44 (Fig. 6b), which are lower values than those of the metasediment-hosted samples (IR27 and IR28) (Fig. 6a).

X-HCO_3 type samples whose host rocks are metasediments are all collected from the albite-biotite zone (IR28 and SD09). They show Li/B values of 0.36 and 0.09, and are plotted on the B-Li side. X-HCO_3 type fluids of mafic rocks also show a wide Li/B range (0.02–0.19) irrespective of the metamorphic grade of the host rock, which is slightly lower than those of the metasediments.

Intermediate type samples (WS02 and 07113002) are found only in mafic-rock-hosted veins, as mentioned above, and have relatively higher-Cl ratios compared to Na-Cl and X-HCO_3 type samples (Fig. 6b).

As an overall trend, all crush-leached fluids from quartz veins show very high (B+Li)/Cl compositions, though some fluid inclusions were certainly entrapped during the later stage of the exhumation of the rock. Li/B ratios of the fluid seem to vary depending on several factors such as host rock lithology, quartz grain fabric (deformation history), and metamorphic grade. However, P-type samples collected from high-metamorphic-grade parts, i.e. samples expected to retain the fluid in the deep part of the subduction zone, have a tendency to show a high content of both Li and B. One typical example of high saline, Li- and B-enriched fluid is IR27 collected from the oligoclase-biotite zone, which contains predominant type 2B inclusions (IR27a) and a very small amount of IR27b (type undetermined: Table 2), and thus, the composition of the crush-leached fluid are expected to represent the composition of fluids of IR27a. The Li and B content of crush-leached fluid from IR27 (63.89 and 39.5 μg/L, respectively) are recalculated into the original concentration of fluid inclusions, 348 and 256 μg/g based on the Cl-content and microthermometry results of IR27a. Notably, in metasediment-hosted and mafic rock-hosted samples, respectively, Na-Cl type fluids tend to be high in both Li and B and such Li- and B-enriched fluids are found from higher metamorphic grade part, i.e. the eclogite nappe and its proximal area in central Shikoku.

7. Discussion

7.1. Entrapment Timing of Fluid Inclusions

As fluid inclusions in the common natural sample were generally trapped through the multistage fluid activities which the host metamorphic rock underwent, the extracted fluids obtained by the crush-leach method usually give the integrated result of the whole history of fluid activity. Therefore careful observation of the fluid inclusion textures associated with the deformation texture of the host minerals is necessary to interpret the compositions of crush-leached fluids. Anhydrous type 4 fluid inclusions are thought to have little or no contributions to the chemical composition of crush-leached fluids, although they do provide indispensable information for reconstructing the deep fluid activity that took place in the subduction zone.

To be noted at first, "primary fluid inclusions" *sensu stricto*, which are trapped during the nucleation and crystal growth process of the host minerals (quartz in this study), should be almost absent due to the metamorphic recrystallization in the studied samples. Thus we have to consider the timing of fluid entrapment to be linked to the stage of metamorphism.

The occurrence of fluid inclusions arranged along intragranular planes in P-type veins (Fig. 4a; IR04a/b and SSB04c) suggests that they were trapped before the formation of apparent grain boundaries, i.e. before or during the recrystallization of the host quartz. Thus, they are interpreted as fluid inclusions trapped during the prograde or peak metamorphic stage. P-type textures in the studied samples are equivalent to "foam microstructure" (Stöckhert et al., 1997; Krenn, 2010), and such veins are expected to have escaped from the deformation and corresponding fluid infiltration during the later stage of exhumation. Therefore fluid inclusions arranged along transgranular planes in P-type veins also would have been trapped during the peak metamorphic stage or early stage of exhumation with relatively high temperatures. For IR04 and IR27, we have also reported that the formation of these textures took place near the peak metamorphic stage or at the early stage of

exhumation (Yoshida et al., 2011; Yoshida & Hirajima, 2012). Furthermore, Yoshida and Hirajima (2012) also found annular shaped fluid inclusions in IR04 (IR04a) and concluded that they were trapped at the prograde stage of the metamorphism.

On the other hand, fabrics of DI- and DD-type, represented by largely deformed lamellae and undulatory extinction (Figs. 3c/d), are thought to be formed under high differential stress and relatively low temperature (<400 ºC) (Passchier & Trouw, 2005). Given the metamorphic history of the Sanbagawa metamorphic belt, such conditions are expected for the large scale deformation event during the later stage of exhumation (e.g., Mori and Wallis, 2010 and references therein). Fluid inclusions arranged along transgranular planes of DI-/DD-type veins are thought to be trapped in association with the later-stage deformation event and corresponding fluid infiltration. However, the exact timings of fluid infiltration have not been determined.

Fluid inclusions in the chlorite zone sample (WS04) and later-stage vein (10AS18) are arranged at subgrain boundaries (Fig. 4e). Such fluid inclusion arrays may have been trapped in conjunction with the recrystallization of host quartz veins under high differential stress. Such conditions are expected to occur at both peak metamorphic stage of the chlorite zone (300^{o}C/ 0.5 GPa) and the later exhumation stage.

In conclusion, P-type veins are capable of retaining fluids trapped at pre-peak metamorphic stages, and further of containing fluid inclusions trapped at the peak metamorphic stage or early stage of exhumation. DI-/DD-type veins have trapped post-peak metamorphic fluid during the exhumation stage, except for WS04, since we cannot distinguish the conditions of the peak metamorphic stage of the chlorite zone and the exhumation stage.

7.2. Hydrochemical characteristics

The results of ion chromatography and ICP-MS analysis presented here (Table 3) can provide fruitful

information to constrain the nature of deep fluids trapped at ca. 15 km to 60 km depths. Samples containing type 2 or 3 fluid inclusions (relatively higher salinity fluids) tend to be characterized by Na-Cl type hydrochemical characteristics, i.e. three samples (IR27, IR04 and SSB03) are Na-Cl type (Fig. 5). On the other hand, samples free from type 2 and type3 fluid inclusions, i.e. only the dilute fluid bearing sample in this study, show both Na-Cl type and X-HCO_3 type fluids.

These features are closely correlated with the fabrics of quartz grains in the vein: five P-type veins (out of six) are Na-Cl type and all DI- and DD-type veins are intermediate or X-HCO_3 type (Fig. 5). The later stage vein (10AS18) shows the most HCO_3-rich composition. Dominance of HCO_3 is known to be characteristic of pore fluids in near surface fracture of continental crust (Bucher & Stober, 2010) thus, HCO_3-dominated composition probably indicates shallow-depth fluids that have infiltrated during the later stage of exhumation of the Sanbagawa belt.

In a review, Yardley and Graham (2002) pointed out that there is scarce correlation between metamorphic grade and salinity of corresponding fluid inclusions. They also suggested that fluid inclusions hosted in metamorphic rocks originated from oceanic crust or accretionary prisms would be relatively dilute fluid compared to those in metamorphic rocks derived from the continent crustal materials. They indicated that there was a large variation in the salinity of such fluids, from up to 15 mass%$_{NaCleq}$ to mostly solute free for relatively high metamorphic grades (400–700 ºC). Gao and Klemd (2001) also reported that aqueous fluids released by blueschist-eclogite transition reaction in Tianshan, China, have low salinities. Our data present here also show scarce correlation between salinity, halogen content of minerals (Table S1-S3), and metamorphic grades/entrapment timing, however, the P-type veins tend to have relatively high-saline fluid inclusions.

In this study, a correlation between quartz fabric types in the veins and hydrochemical characteristics is observed, i.e. P-type quartz veins tends to contain Na-Cl type fluid, and DI- and DD-type quartz veins tend to have X-HCO_3 type fluids. This correlation suggests that Na-Cl type fluids are more likely to be produced at deeper parts of subduction zones, and X-HCO_3 type fluids

are likely to be produced at depths shallower than 15 km, which are defined by the peak *P-T* conditions (300ºC/ 0.5 GPa) of the chlorite zone. High-saline aqueous fluid can be generated by the preferential water consumption due to the hydration of the water-unsaturated rock (e.g., Scambelluri et al., 1997; John and Schenk, 2003). However, the compositions of the hydrous minerals in host metamorphic rocks (Table S1-S3) show scarce amount of the Cl content and therefore do not intimate the hydration reaction as the origin of the high-salinity of aqueous fluid. The controlling factors of salinities in fluid inclusions still remain unclear in this study.

7.3. Volatile component of fluid inclusions

Aqueous fluid inclusions investigated in this study are commonly accompanied with N_2 and/or CH_4 (ten samples out of eleven). Chemical compositions of crush-leached fluids also suggest X-HCO_3 and intermediate type samples contain significant amount of HCO_3. We further observed type 4 anhydrous fluid inclusion groups with (SD09a, SSB04c, IR04b) or without (IR28a, SSB03b) CO_2 component. Although there is a possibility that type 4 fluid inclusions contain a small amount of water undetectable by ordinary Raman microscopy at room temperature, the amount of water should be less than a few mol% (e.g., Berkesi et al., 2009) and can be negligible for most discussion.

The origin of N_2 in metamorphic rocks is considered to be the oxidation reaction of NH_4-bearing mica and/or feldspar (e.g., Anderson et al., 1993), while that of CH_4 is considered to be the reductive reaction of CO_2 or thermal cracking of organic materials (e.g., Mazurek, 1999; Herms et al., 2012). Fluid inclusions with CO_2 are commonly reported from high grade metamorphic rocks in the world (e.g., Kobayashi et al., 2011) and also from mantle rocks (e.g., Yamamoto et al., 2007). H_2O-NaCl-CH_4 fluid are reported as the peak metamorphic stage fluid of the chlorite zone of the Sanbagawa belt (Nishimura et al., 2008) and as the prograde stage fluid of the sample IR04 (Yoshida and Hirajima, 2012), although Yoshida and Hirajima (2012) did not constrain the *P-T* condition of the entrapment of H_2O-NaCl-CH_4 fluid (IR04a). Thus, at the low to medium grade part of the

Sanbagawa metamorphic belt, the existence of H_2O-NaCl-CH_4 fluid is expected. Volatile-free aqueous fluid of WS04 could be similar to the exhumation stage fluid of the chlorite zone reported by Okamoto et al. (2008), which is possibly trapped at early stage of the exhumation. Since WS02 from the garnet zone sample and higher grade samples commonly contain N_2-bearing fluid, N_2 is a ubiquitous species at greater depth than ca. 15 km. In the higher metamorphic grade samples, all CH_4-bearing aqueous fluids are free from CO_2. At high oxidation state, the oxidation reaction of CH_4 and H_2O can generate CO_2. Dissolved HCO_3 in X-HCO_3 type fluid (SD09, IR28: Fig. 5) with CH_4 are possibly originated from the partial oxidation of CH_4. Nevertheless, existence of CO_2-free, HCO_3-poor and CH_4-bearing aqueous fluid suggests that the maximum oxidation states of the high grade samples were not so high as to consume all of CH_4.

SD09 from the albite-biotite zone and SSB04 and IR04 from the eclogite facies rocks contain anhydrous CO_2-CH_4-bearing fluids. Carbon-rich anhydrous fluids are possibly originated from decarbonation of the carbonate minerals. Above-mentioned prograde CH_4-bearing fluids are also available for the carbon source. All type 4 fluids are obtained from the higher grade samples than the albite-biotite zone, suggesting such anhydrous fluids are expected at deeper part.

Nevertheless, detailed discussion on the evolutional changes of carbon and other volatile species is beyond the purpose of this paper.

7.4. Relative B-Li-Cl Compositions

The crush-leached fluids of this study are characterized by high B and Li content, corresponding to very high (B+Li)/Cl ratios, though microthermometry results suggest some of them have higher Cl content than modern seawater. Among the studied samples, WS02 and 07113002, whose crush-leached fluids have intermediate type hydrochemical characteristics, show slightly lower (B+Li)/Cl compositions. For comparison, relative B-Li-Cl compositions of hydrothermal and metamorphic fluids in the literatures are compiled in figures 6c and 6d (Scambelluri et al., 2004; Ohsawa et al.,

2010; Kazahaya et al., 2014). The modern seawater and squeezed pore water from marine sediments (Ohsawa et al., 2010) show low (B+Li)/Cl compositions (Fig. 6d). If such fluid infiltrated into the Sanbagawa metamorphic terrane and was trapped in quartz veins during the exhumation stage, the compositions of crush-leached fluids can be modified towards the Cl-corner of the diagram. However, this effect is scarce or limited for all the studied samples (Fig. 6a/b).

Crush-leached fluids are enriched in B and Li compared to modern seawater, but have a large variation in their Li/B ratio, ranging from 0.02 (WS04) to 1.99 (IR04). Dehydration fluids from serpentinites trapped in metamorphic olivine grains (400–700 ºC, 1.5–2.5 GPa: Scambelluri et al., 2004) have very high Li/B ratios (>2) and show large variation in their Li/Cl ratio (Fig. 6c). Scambelluri et al. (2004) estimated the partition coefficients between serpentinite and fluids at eclogite facies conditions based on their geochemical measurement and mass balance calculations, resulting in $D^{rock/fluid}_{Cl}$ =0.01–0.02 and $D^{rock/fluid}_{B}$ =0.02–0.04 as first approximation. Based on their mass balance calculation, the B/Cl ratio of the dehydrated fluid from serpentinite will be 0.04–0.16 (dashed-lined area in Fig. 6c), overlapping the range of our data (Fig. 6a/b).

Ohsawa et al. (2010) reported high B/Cl and low Li/B ratio fluids from the hot spring waters in the Miyazaki plain located in the fore-arc region of Kyushu Island, SW Japan (Fig. 6d). Based on the geochemical data combined with geochemical thermometry, they indicated that high B/Cl and low Li/B fluids are derived from dehydration of smectite interlayers. Ohsawa et al. (2010) and Amita et al. (2014) also reported relative B-Li-Cl compositions of hot spring waters obtained from deep wells in the fore-arc region of southwest Japan (S1, S2, O1, O2, and W in Fig. 6d). They proposed that diagenetic/metamorphic fluids show an evolutionary trend of increasing B/Cl ratio along the Cl-B axis and subsequent increase of the Li/B ratio with progressive diagenetic/metamorphic processes.

Recently, Kazahaya et al. (2014) investigated the isotopic and chemical compositions of hot spring waters in SW Japan and proposed that Arima-type hydrothermal fluids (e.g., Matsubaya et al., 1973) have Li/Cl ratios higher than 0.001 (shown in Fig. 6d) and high salinities (Cl >200 mg/L). The

Arima-type hydrothermal fluids show high salinity, $\delta^{18}O$ value, and $^{3}He/^{4}He$ ratio with low δD compared to the modern sea water. Kusuda et al. (2014) investigated geochemical characteristics of Arima-type hydrothermal fluids of the Arima-Takarazuka area, SW Japan. On the basis of the isotopic data ($\delta^{18}O$ and δD values), they indicated that Arima-type hydrothermal fluids in that area are originated from the subducting slab locating at approximately 60 km depth beneath the land surface.

All of these studies suggest that a certain amount of fluids achieved upwelling from the deep part of the subduction zone (e.g., at least 50-60 km depths) and their compositions are characterized by high (B+Li)/Cl ratios.

Enrichment of Li and B is partly explained by the partition coefficient data (Brenan et al., 1998; Tenthorey & Hermann, 2004; Marschall et al., 2006). We calculated the bulk partition coefficient for our samples from the mineral abundances and partition coefficients of Marschall et al. (2006) (Fig. 7), showing that most partition coefficient pairs are much lower than 1.

Published partition coefficient data of B and Li between whole rock and aqueous fluids are also shown in figure 7. The data of Kessel et al. (2005) have been obtained experimentally for K-free MORB compositions, including a *T* range of 700–900ºC at 4GPa. Marschall et al. (2007) estimated the partition coefficients of altered oceanic crust subducting along the *P*-*T* path of relatively cold slab (~ 3.8 MPa/ºC). Yoshida et al. (2011) also calculated partition coefficients for the bulk composition of a specific pelitic schist along the metamorphic field gradient of the Sanbagawa belt (1.64 MPa/ºC, Enami et al., 1994), following the method of Marschall et al. (2007). Figure 7 shows that, in most cases, $D_{Li}^{rock/fluid}$ and $D_{B}^{rock/fluid}$ show a value lower than 1, suggesting these elements would be released from the rock during water-rock interaction (e.g., Marschall et al., 2006). Since we have not measured the whole rock concentration of Li and B, let us assume that Li and B concentration of the high-pressure type metasedimentary rocks are 50-100 μg/g and 20-150 μg/g, respectively (e.g., Bebout et al., 2013; Nakano and Nakamura, 2001). If these rocks are equilibrated with the crush-

leached fluid (e.g., IR27: 348 μg/g for Li and 256 μg/g for B), partition coefficients would be $D_{Li}^{rock/fluid}$ = 0.2-0.3 and $D_{B}^{rock/fluid}$ = 0.08-0.6. $D_{Li}^{rock/fluid}$ is higher than previously estimated values, while $D_{B}^{rock/fluid}$ falls in a mostly similar range (Fig. 7).

7.5. Implications for light element cycles in the subduction zone

The fluid chemistry discussed above suggests that fluid activity, which is characterized by relatively high-saline aqueous fluid (5–10 mass%$_{NaCleq}$) with B- and Li-enriched compositions (up to ~300 μg/g), could be predominant at certain depths in the subduction zone. Nevertheless, there is a large variation in the salinity and Li/B ratio of the fluids. Release of high-saline and B-Li-enriched fluids beneath the subduction zone can supply these elements to the hanging walls of the subducting slab, such as accretionary prisms and continental crust in the shallow part of the subduction zone, and/or the mantle wedge in the deeper part. Marschall et al. (2009) investigated a metasomatized H*P* metamorphic suite in Syros, Greece and indicated that the whole rock Li abundance of the H*P* metamorphic rocks would increase with metasomatic process, i.e. metasomatic agents would have a high Li content. The high-saline and Li-enriched fluids observed in this study, i.e. the most typical samples, IR04 and IR27, have the potential to explain the origin of these high-Li metasomatic agents.

Some bulk trace elements studies on the successive metamorphic suites indicate that most of Li and B are retained in the rock during progressive dehydration and corresponding water-rock interaction, because of the redistribution of these elements among the suitable minerals. On the basis of the whole rock analysis of a series of samples collected from the Catalina Schist covering from lawsonite-albite facies to amphibolite facies, Penniston-Dorland et al. (2012) pointed out that the whole rock concentration of lithium is controlled by the content of Al_2O_3, corresponding to the modal amount of phengite and chlorite. Nakano and Nakamura (2001) studied pelitic schists covering from pumpellyite-actinolite facies to epidote-amphibolite facies and indicated that progressive releasing of boron from chlorite and phengite are *in situ* consumed by coarsening of

tourmaline. Bebout et al. (2013) also indicate the *in situ* consumption of released lithium and boron in the pelitic schists, covering from blueschist facies conditions to ultra-high pressure conditions. Let us consider the impact of the releasing of B- and Li-enriched fluid during the progressive dehydration of subducting materials, by a simple calculation. If we assume a dehydrated aqueous fluid with 300 μg/g of B and Li, and the removed amount of the fluid is as high as 3 mass% of the rock, the loss of B and Li would be only 9 μg/g. This value is considerably small compared to above-mentioned bulk concentration of the high-pressure type metasedimentary rocks (20-150 μg/g). Therefore, most B and Li are retained within the solid phases. Dehydration of 3 mass% are almost highest limit of the dehydration amount of the high-pressure metamorphic rocks under 300-700 ºC (e.g., Hacker et al., 2008; Bebout et al., 2013), and thus, these element losses could be the highest estimation. This simple calculation indicates that removal of the B- and Li-rich fluids at high-pressure conditions do not largely invoke the B- and Li-loss of the bulk rock system because of the small amount of the dehydrated fluids. However, these B- and Li-rich fluids can be released from the metamorphic rocks and would invoke some significant geochemical signal at the hanging wall of the subduction zone.

Acknowledgements

This work was partly supported by the JSPS (Grant-in-Aid for JSPS Fellows for KY, No. 25-57, Grant-in Aid for Scientific Research Nos. 25257208 and 22244067, and Grand-in Aid for Innovative Areas 2018 “Geofluid”) and by Nozomi Farm, Ltd. We also would like to thank T. Kawakami, F. Higashino, S. Tsuchiya, and K. Minagawa in Petrological group of Kyoto University for their fruitful discussions. This paper benefited from constructive reviews by J. Hermann and an anonymous reviewer, and the editorial handling by D. Castelli.

References

Amita, K., Ohsawa, S., Nishimura, K., Yamada, M., Mishima, T., Kazahaya, K., Morikawa, N. & Hirajima, T., 2014. Origin of saline waters distributed along the Median Tectonic Line in southwest Japan: Hydrogeochemical investigation on possibility of derivation of metamorphic dehydrated fluid from subducting oceanic plate. Journal of Japanese Association of Hydrological Sciences, 44, 17–38.

Anderson, T., Austrheim, H., Burke, E. A. J. & Elvevold, S., 1993. N_2 and CO_2 in deep crustal fluids: evidence from the Caledonides of Norway. Chemical Geology, 108, 113-132.

Aoya, M., 2001. P–T–D path of eclogite from the Sambagawa belt deduced from combination of petrological and microstructural analyses. Journal of Petrology, 42, 1225–1248.

Aoya, M., Endo, S., Mizukami, T. & Wallis, S. R., 2013. Paleo-mantle wedge preserved in the Sambagawa high-pressure metamorphic belt and the thickness of forearc continental crust. Geology, 41, 451–454.

Aoya, M., Noda, A., Mizuno, K., Mizukami, T., Miyachi, Y., Matsuura, H., Endo, S., Toshimitsu, S. & Aoki, M., 2013. Geology of the Niihama District. Quadrangle Series, 1 :50,000, Geological Survery of Japan, AIST.

Bakker, R. J. & Mamtani, M. A., 2000. Fluid inclusions as metamorphic process indicators in the Southern Aravalli Mountain Belt (India). Contributions to Mineralogy and Petrology, 139, 163–179.

Banks, D. A. & Yardley, B. W. D., 1992. Crush-leach analysis of fluid inclusions in small natural and synthetic samples. Geochimica et Cosmochimica Acta, 56, 245–248.

Bebout, G. E., 2007. Metamorphic chemical geodynamics of subduction zones. Earth and Planetary Science Letters, 260, 373–393.

Bebout, G. E., Ryan, J. G. & Leeman, W. P., 1993. B-Be systematics in subduction-related metamorphic rocks: Characterization of the subducted component. Geochimica et Cosmochimica Acta, 57, 2227–2237.

Bebout, G. E., Ryan, J. G., Leeman, W. P. & Bebout, A. E., 1999. Fractionation of trace elements by subduction - zone metamorphism - effect of convergent-margin thermal evolution. Earth and Planetary Science Letters, 171, 63–81.

Bebout, G. E., Agard, P., Kobayashi, K., Moriguti, T. & Nakamura, E., 2013. Devolatilization history and trace element mobility in deeply subducted sedimentary rocks: Evidence from Western Alps HP/UHP suites. Chemical Geology, 342, 1-20.

Berkesi, M., Hidas, K., Guzmics, T., Dubessy, J., Bodnar, R. J., Szabo, C., Vajna, B. & Tsunogae, T., 2009. Detection of small amounts of H2O in CO2‐rich fluid inclusions using Raman spectroscopy. Journal of Raman Spectroscopy, 40, 1461-1463.

Bodnar, R. J., 1993. Revised equation and table for determining the freezing point depression of H2O-NaCl solutions. Geochimica et Cosmochimica Acta, 57, 683–684.

Bottrell, S. H., Yardley, B. W. D. & Buckley, F., 1988. A modified crush-leach method for the analysis of fluid inclusion electrolytes. Bulletin de minéralogie, 111, 279–290.

Boullier, A.-M., 1999. Fluid inclusions: tectonic indicators. Journal of Structural Geology, 21, 1229–1235.

Brenan, J. M., Ryerson, F. J. & Shaw, H. F., 1998. The role of aqueous fluids in the slab-to-mantle transfer of boron, beryllium, and lithium during subduction: experiments and models. Geochimica et Cosmochimica Acta, 62, 3337–3347.

Bucher, K. & Stober, I., 2010. Fluids in the upper continental crust. Geofluids, 241–253.

Caciagli, N., Brenan, J. M., McDonough, W. . & Phinney, D., 2011. Mineral–fluid partitioning of lithium and implications for slab–mantle interaction. Chemical Geology, 280, 384–398.

Domanik, K. J., Hervig, R. L. & Peacock, S. M., 1993. Beryllium and boron in subduction zone minerals: An ion microprobe study. Geochimica et Cosmochimica Acta, 57, 4997–5010.

Donnelly, T. W., Thompson, G. & Salisbury, M. H., 1980. The chemistry of altered basalts at site 417, Deep Sea Drilling Project Leg 75. Institute Report of DSPS, 51-53, 1319–1330.

Enami, M., 1982. Oligoclase-biotite zone of the Sanbagawa metamorphic terrain in the Bessi district, central Shikoku, Japan. Journal of Geological Society of Japan, 88, 887–900.

Enami, M., 1994. Sanbagawa metamorphism: Implication for evolution of a subduction zone. Japanese Magazine of Mineralogical and Petrological Sciences, 89, 409–422.

Endo, S., 2010. Pressure-temperature history of titanite-bearing eclogite from the Western Iratsu body, Sanbagawa Metamorphic Belt, Japan. Island Arc, 19, 313–335.

Endo, S., Wallis, S. R., Tsuboi, M., Torres De León, R. & Solari, L. a., 2012. Metamorphic evolution of lawsonite eclogites from the southern Motagua fault zone, Guatemala: insights from phase equilibria and Raman spectroscopy. Journal of Metamorphic Geology, 30, 143–164.

Gao, J. & Klemd, R., 2001. Primary fluids entrapped at blueschist to eclogite transition: evidence from the Tianshan meta-subduction complex in northwestern China. Contributions to Mineralogy and Petrology, 142, 1–14.

Hacker, B. R., 2008. H_2O subduction beyond arcs. Geochemistry Geophysics Geosystems, 9, Q03001, doi:10.1029/2007GC001707.

Higashino, F., Kawakami, T., Satish-Kumar, M., Ishikawa, M., Maki, K., Tsuchiya, N., Grantham, G. H. & Hirata, T., 2013. Chlorine-rich fluid or melt activity during granulite facies metamorphism in the Late Proterozoic to Cambrian continental collision zone—An example from the Sør Rondane Mountains, East Antarctica. Precambrian Research, 234, 229–246.

Higashino, T., 1990. The higher grade metamorphic zonation of the Sambagawa metamorphic belt in central Shikoku, Japan. Journal of Metamorphic Geology, 8, 413–423.

Jarrard, R. D., 2003. Subduction fluxes of water, carbon dioxide, chlorine, and potassium. Geochemistry Geophysics Geosystems, 4, doi: 10.1029/2002GC000392

John, T. & Schenk, V., 2003. Partial eclogitisation of gabbroic rocks in a late Precambrian subduction zone (Zambia): prograde metamorphism triggered by fluid infiltration. Contributions to Mineralogy and Petrology, 146, 174-191.

Kazahaya, K., Takahashi, M., Yasuhara, M., Nishio, Y., Inamura, A., Morikawa, N., Sato, T., Takahashi, H. a., Kitaoka, K., Ohsawa, S., Oyama, Y., Ohwada, M., Tsukamoto, H., Horiguchi, K., Tosaki, Y., Kirita, T., 2014. Spatial distribution and feature of slab-related deep-seated fluid in SW Japan. Journal of Japanese Association of Hydrological Sciences 44, 3–16.

Van den Kerkhof, A., 2001. Fluid inclusion petrography. Lithos, 55, 27–47.

Kessel, R., Schmidt, M. W., Ulmer, P. & Pettke, T., 2005. Trace element signature of subduction-zone fluids, melts and supercritical liquids at 120-180 km depth. Nature, 437, 724–7.

Kobayashi, T., Hirajima, T., Kawakami, T., Svojtka, M., 2011. Metamorphic history of garnet-rich gneiss at Ktiš in the Lhenice shear zone, Moldanubian Zone of the southern Bohemian Massif, inferred from inclusions and compositional zoning of garnet. Lithos, 124, 46-65.

Kogiso, T., Tatsumi, Y. & Nakano, S., 1997. Trace element transport during dehydration processes in the subducted oceanic crust: 1. Experiments and implications for the origin of ocean island basalts. Earth and Planetary Science Letters, 148, 193–205.

Konrad-Schmolke, M., O'Brien, P. J. & Zack, T., 2011. Fluid Migration above a Subducted Slab--Constraints on Amount, Pathways and Major Element Mobility from Partially Overprinted Eclogite-facies Rocks (Sesia Zone, Western Alps). Journal of Petrology, 52, 457–486.

Kouketsu, Y., Enami, M. & Mizukami, T., 2010. Omphacite-bearing metapelite from the Besshi region, Sambagawa metamorphic belt, Japan: Prograde eclogite facies metamorphism recorded in metasediment. Journal of Mineralogical and Petrological Sciences, 105, 9–19.

Kouketsu, Y., Enami, M., Mouri, T., Okamura, M., Sakurai, T., 2014. Composite metamorphic history recorded in garnet porphyroblasts of Sambagawa metasediments in the Besshi region, central Shikoku, Southwest Japan. Island Arc, 23, 263-280..

Krenn, K., 2010. Fluid inclusions in quartz related to subsequent stages of foliation development during a single metamorphic cycle (Schneeberg Fault Zone, Eastern Alps, Austria). Lithos, 118, 255–268.

Krenn, K., Bauer, C., Proyer, A., Mposkos, E. & Hoinkes, G., 2008. Fluid entrapment and reequilibration during subduction and exhumation: A case study from the high-grade Nestos shear zone, Central Rhodope, Greece. Lithos, 104, 33–53.

Kunugiza, K., Takasu, A. & Banno, S., 1986. The origin and metamorphic history of the ultramafic and metagabbro bodies in the Sanbagawa belt. Geological Society of America Memoir, 164, 375–385.

Kurata, H. & Banno, S., 1974. Low-grade progressive metamorphism of pelitic schists of the Sazare area, Sanbagawa metamorphic terrain in central Sikoku, Japan. Journal of Petrology, 15, 361–382.

Kusuda, C., Iwamori, H., Nakamura, H., Kazahaya, K. and Morikawa, N. (2014) Arima hot spring waters as a deep-seated brine from subducting slab. Earth, Planets and Space, 66, 119.

Küster, M. & Stöckhert, B., 1997. Density changes of fluid inclusions in high-pressure low-temperature metamorphic rocks from Crete: A thermobarometric approach based on the creep strength of the host minerals. Lithos, 41, 151–167.

Leeman, W. P. & Sisson, V. B., 1996. Geochemistry of boron and its implications for crustal and mantle processes. Reviews in Mineralogy and Geochemistry, 33, 645–707.

Makimoto, H., Miyata, T., Mizuno, K. & Sangawa, A., 2004. Geology of the Kokawa District. Quadrangle Series, 1 :50,000, Geological Survery of Japan, AIST.

Marschall, H. R., Altherr, R., Gméling, K. & Kasztovszky, Z., 2009. Lithium, boron and chlorine as tracers for metasomatism in high-pressure metamorphic rocks: a case study from Syros (Greece). Mineralogy and Petrology, 95, 291–302.

Marschall, H. R., Altherr, R., Ludwig, T., Kalt, A., Gméling, K. & Kasztovszky, Z., 2006. Partitioning and budget of Li, Be and B in high-pressure metamorphic rocks. Geochimica et Cosmochimica Acta, 70, 4750–4769.

Marschall, H. R., Altherr, R. & Rüpke, L., 2007. Squeezing out the slab–modelling the release of Li, Be and B during progressive high-pressure metamorphism. Chemical Geology, 239, 323–335.

Marschall, H. R., Korsakov, a. V., Luvizotto, G. L., Nasdala, L. & Ludwig, T., 2009. On the occurrence and boron isotopic composition of tourmaline in (ultra)high-pressure metamorphic rocks. Journal of the Geological Society, 166, 811–823.

Matsubaya, O., Sakai, H., Kusachi, I. & Satake, H., 1973. Hydrogen and oxygen isotopic ratios and major element chemistry of Japanese thermal water systems. Geochemical Journal, 7, 123–151.

Matsumoto, K. & Hirajima, T., 2006. Modal analysis using scanning electron probe microanalyzer. Japanese Magazine of Mineralogical and Petrological Sciences, 35, 97–108.

Mazurek, M., 1999. Evolution of gas and aqueous fluid in low-permeability argillaceous rocks during uplift and exhumation of the central Swiss Alps. Applied Geochemistry, 15, 211-234.

Mori, H. & Wallis, S., 2010. Large-scale folding in the Asemi-gawa region of the Sanbagawa Belt, southwest Japan. Island Arc, 19, 357–370.

Nakano, T. & Nakamura, E., 2001. Boron isotope geochemistry of metasedimentary rocks and tourmalines in a subduction zone metamorphic suite. Physics of The Earth and Planetary Interiors, 127, 233–252.

Newton, R. C. & Manning, C. E., 2010. Role of saline fluids in deep-crustal and upper-mantle metasomatism: insights from experimental studies. Geofluids, 58–72.

Nishimura, K., Amita, K., Ohsawa, S., Kobayashi, T. & Hirajima, T., 2008. Chemical characteristics and trapping P-T conditions of fluid inclusions in quartz veins from the Sanbagawa metamorphic belt, SW Japan. Journal of Mineralogical and Petrological Sciences, 103, 94–99.

Ohsawa, S., 2004. Geochemical characteristics of carbonated brines along Median Tectonic Line, South-west Japan: implication for upward migration of dehydrated-fluid from subducting Philippine Sea plate. 2nd KAGI21 International Symposium Beppu, 2004 Proceeding. B-Con Plaza, Beppu city, Oita, Japan, pp. 45–46.

Ohsawa, S., Amita, K., Yamada, M., Mishima, T. & Kazahaya, K., 2010. Geochemical features and genetic process of hot-spring waters discharged from deep hot-spring wells in the Miyazaki Plain, Kyushu Island, Japan: Diagenetic dehydrated fluid as a source fluid of hot-spring water. Journal of Hot Spring Science, 59, 295–319.

Ota, T., Terabayashi, M. & Katayama, I., 2004. Thermobaric structure and metamorphic evolution of the Iratsu eclogite body in the Sanbagawa belt, central Shikoku, Japan. Lithos, 73, 95–126.

Passchier, C. W. & Trouw, R. A. J., 2005. Microtectonics 2nd Ed., Heidelberg, Berlin: Springer-Verlag.

Peacock, S. M., 1990. Fluid processes in subduction zones. Science, 248, 329–337.

Penniston-Dorland, S. C., Bebout, G. E., Pogge von Strandmann, P. A., Elliott, T. & Sorensen, S. S., 2012. Lithium and its isotopes as tracers of subduction zone fluids and metasomatic processes: Evidence from the Catalina Schist, California, USA. Geochimica et Cosmochimica Acta, 77, 530-545.

Piper, A. M., 1944. A graphic procedure in geochemical interpretation of water analyses. Transactions, American Geophysical Union, 25, 914–928.

Scambelluri, M., Piccardo, G. B., Philippot, P., Robbiano, A. & Negretti, L., 1997. High salinity fluid inclusions formed from recycled seawater in deeply subducted alpine serpentinite. Earth and Planetary Science Letters, 148, 485-499.

Scambelluri, M., Müntener, O., Ottolini, L., Pettke, T. T. & Vannucci, R., 2004. The fate of B, Cl and Li in the subducted oceanic mantle and in the antigorite breakdown fluids. Earth and Planetary Science Letters, 222, 217–234.

Seyfried Jr., W. E., Janecky, D. & Mottl, M., 1984. Alteration of the oceanic crust: Implications for geochemical cycles of lithium and boron. Geochimica et Cosmochimica Acta, 48, 557–569.

Shaw, D. M., Vatin-Perignon, N. & Muysson, J. R., 1977. Lithium in spilites. Geochimica et Cosmochimica Acta, 41, 1601–1607.

Stöckhert, B., Massonne, H.-J. & Ursula Nowlan, E., 1997. Low differential stress during high-pressure metamorphism: The microstructural record of a metapelite from the Eclogite Zone, Tauern Window, Eastern Alps. Lithos, 41, 103–118.

Sumino, H., Burgess, R., Mizukami, T., Wallis, S. R., Holland, G. & Ballentine, C. J., 2010. Seawater-derived noble gases and halogens preserved in exhumed mantle wedge peridotite. Earth and Planetary Science Letters, 294, 163–172.

Takasu, A., 1984. Prograde and retrograde eclogites in the Sambagawa metamorphic belt, Besshi district, Japan. Journal of Petrology, 25, 619–643.

Tatsumi, Y., 1989. Migration of fluid phases and genesis of basalt magmas in subduction zones. Journal of Geophysical Research, 94, 4697–4707.

Tenthorey, E. & Hermann, J., 2004. Composition of fluids during serpentinite breakdown in subduction zones: Evidence for limited boron mobility. Geology, 32, 865-868.

Touret, J. L. ., 2001. Fluids in metamorphic rocks. Lithos, 55, 1–25.

Wallis, S. R. & Aoya, M., 2000. A re-evaluation of eclogite facies metamorphism in SW Japan: proposal for an eclogite nappe. Journal of Metamorphic Geology, 18, 653–664.

Whitney, D. L. & Evans, B. W., 2010. Abbreviations for names of rock-forming minerals. American Mineralogist, 95, 185–187.

Yamamoto, J., Kagi, H., Kawakamo, Y., Hirano, N. & Nakamura, M., 2007 Paleo-Moho depth determined from the pressure of CO_2 fluid inclusions: Raman spectroscopic barometry of mantle-and crust-derived rocks. Earth and Planetary Science Letters, 253, 369-377.

Yardley, B. W. D. & Graham, J. T., 2002. The origins of salinity in metamorphic fluids. Geofluids, 2, 249–256.

Yoshida, K. & Hirajima, T., 2012. Annular fluid inclusions from a quartz vein intercalated with metapelites from the Besshi area of the Sanbagawa belt, SW Japan. Journal of Mineralogical and Petrological Sciences, 107, 50–55.

Yoshida, K., Sengen, Y., Tsuchiya, S., Minagawa, K., Kobayashi, T., Mishima, T., Ohsawa, S. & Hirajima, T., 2011. Fluid inclusions with high Li/B ratio in a quartz vein from the Besshi area of the Sambagawa metamorphic belt: implications for deep geofluid evolution. Journal of Mineralogical and Petrological Sciences, 106, 164–168.

You, C. F., Castillo, P. R., Gieskes, J. M., Chan, L. H. & Spivack, A. J., 1996. Trace element behavior in hydrothermal experiments : Implications for fluid processes at shallow depths in subduction zones. Earth and Planetary Science Letters, 140, 41–52.

Zaw, W. K., Enami, M. & Aoya, M., 2005. Chloritoid and barroisite-bearing pelitic schists from the eclogite unit in the Besshi district, Sanbagawa metamorphic belt. Lithos, 81, 79–100.

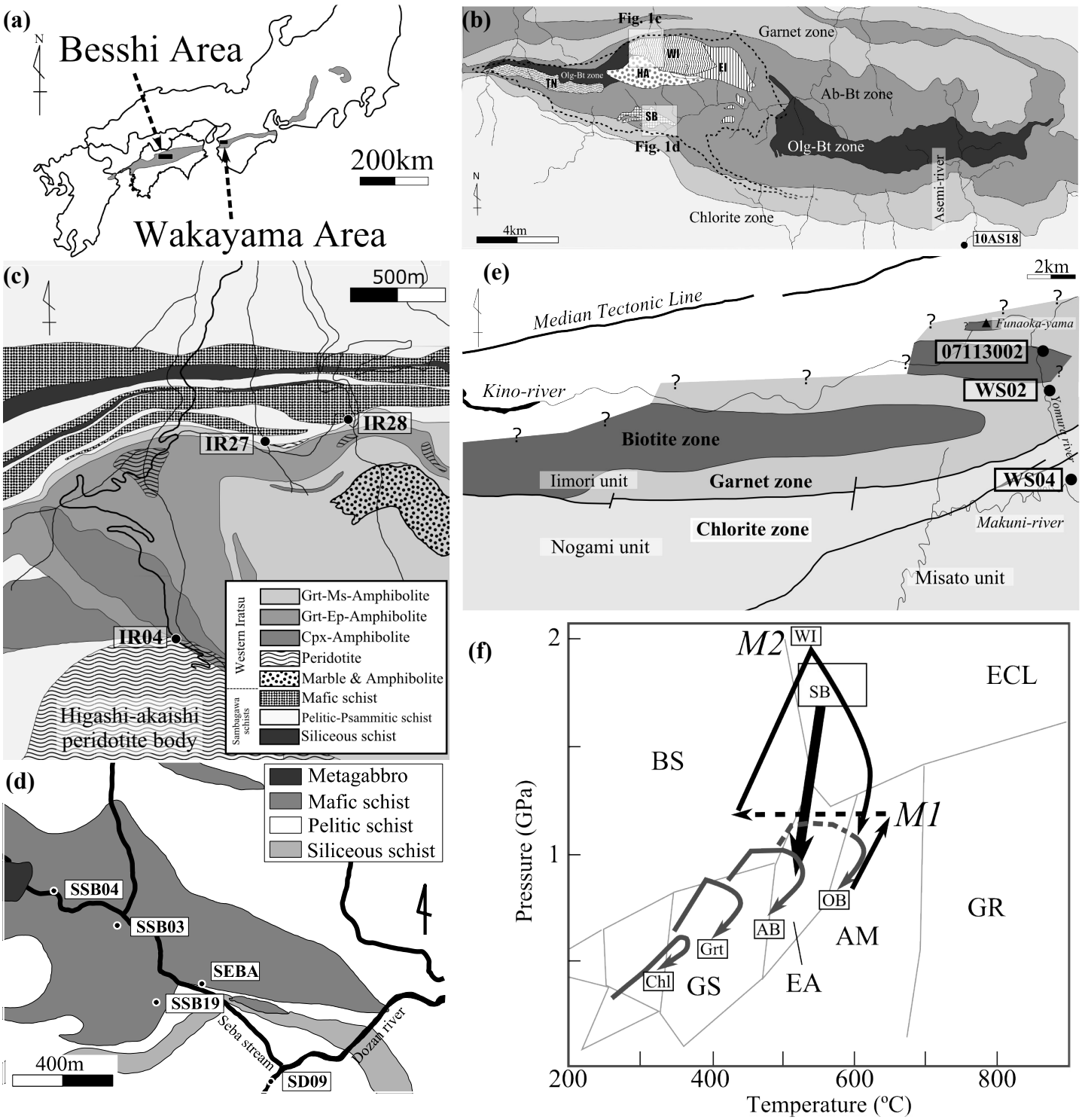

Fig.1. (a) Areal distribution of the Sanbagawa metamorphic belt in SW Japan. (b) Simplified metamorphic zonal map of central Shikoku with the sample locality of the later stage quartz vein collected in the Asemigawa area (10AS18). The dashed line shows the newly proposed boundary of eclogite-nappe in the Besshi area (Aoya et al., 2013); abbreviations of eclogite units are: Tonaru, TN; Seba, SB; Higashi-Akaishi, HA; Western Iratsu, WI; Eastern Iratsu, EI. (c) Lithological map of the study area of the Western Iratsu body (Kugimiya and Takasu, 2002) and sample localities. (d) Lithological map of the study area of the Seba body (Aoya, 2001) and sample localities. (e) Simplified metamorphic zonal map of the Wakayama area after Makimoto et al. (2004) and sampling localities. (f) *P-T* estimation of the Western Iratsu body, Seba body and non eclogitic part of the Sanbagawa metamorphic belt (Enami et al., 1994; Aoya, 2001; Zaw et al., 2005; Endo, 2010).

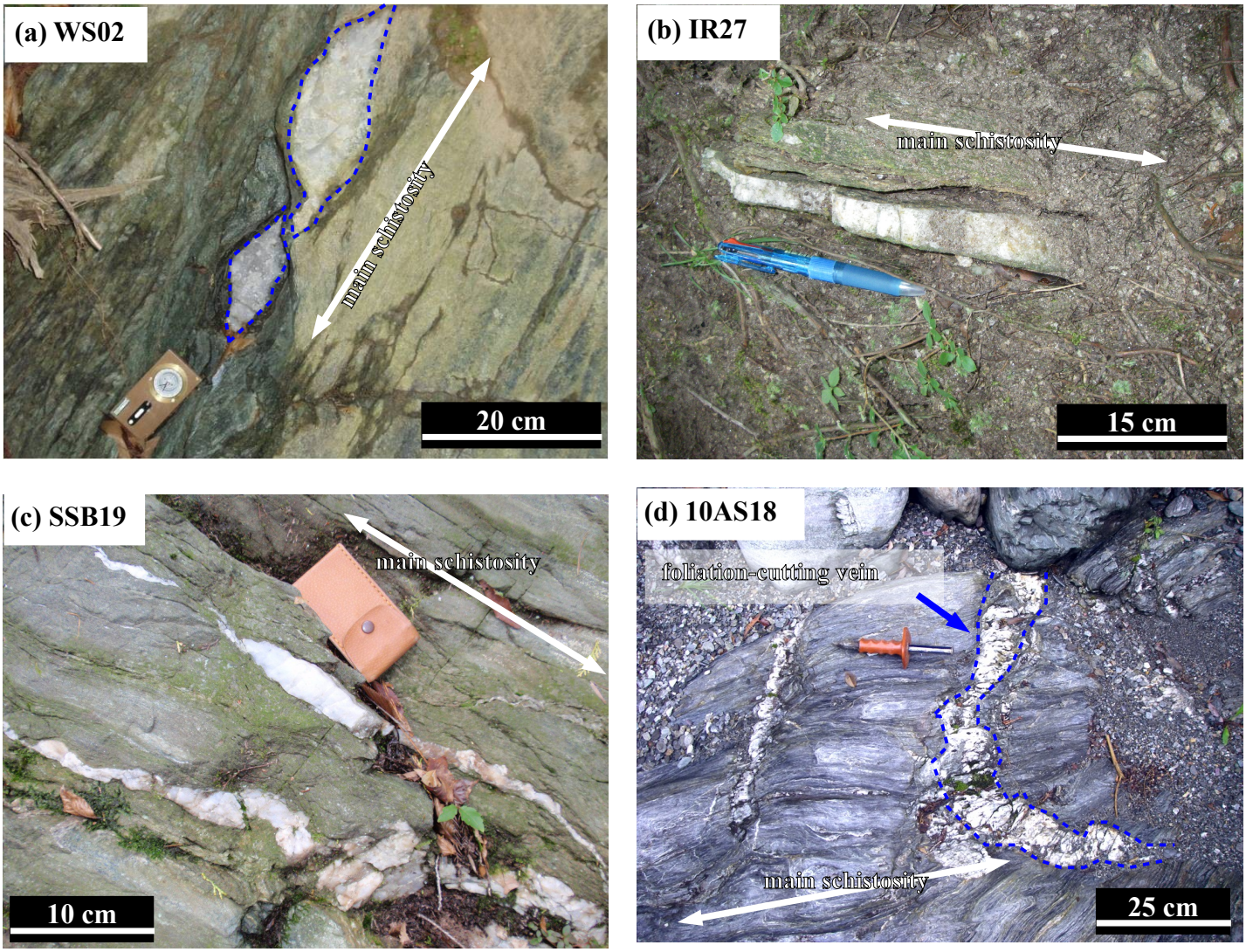

Fig.2. Typical occurrence of (a-c) foliation parallel quartz veins from the Wakayama and Besshi areas; (d) a foliation-cutting vein in the Asemigawa area (10AS18).

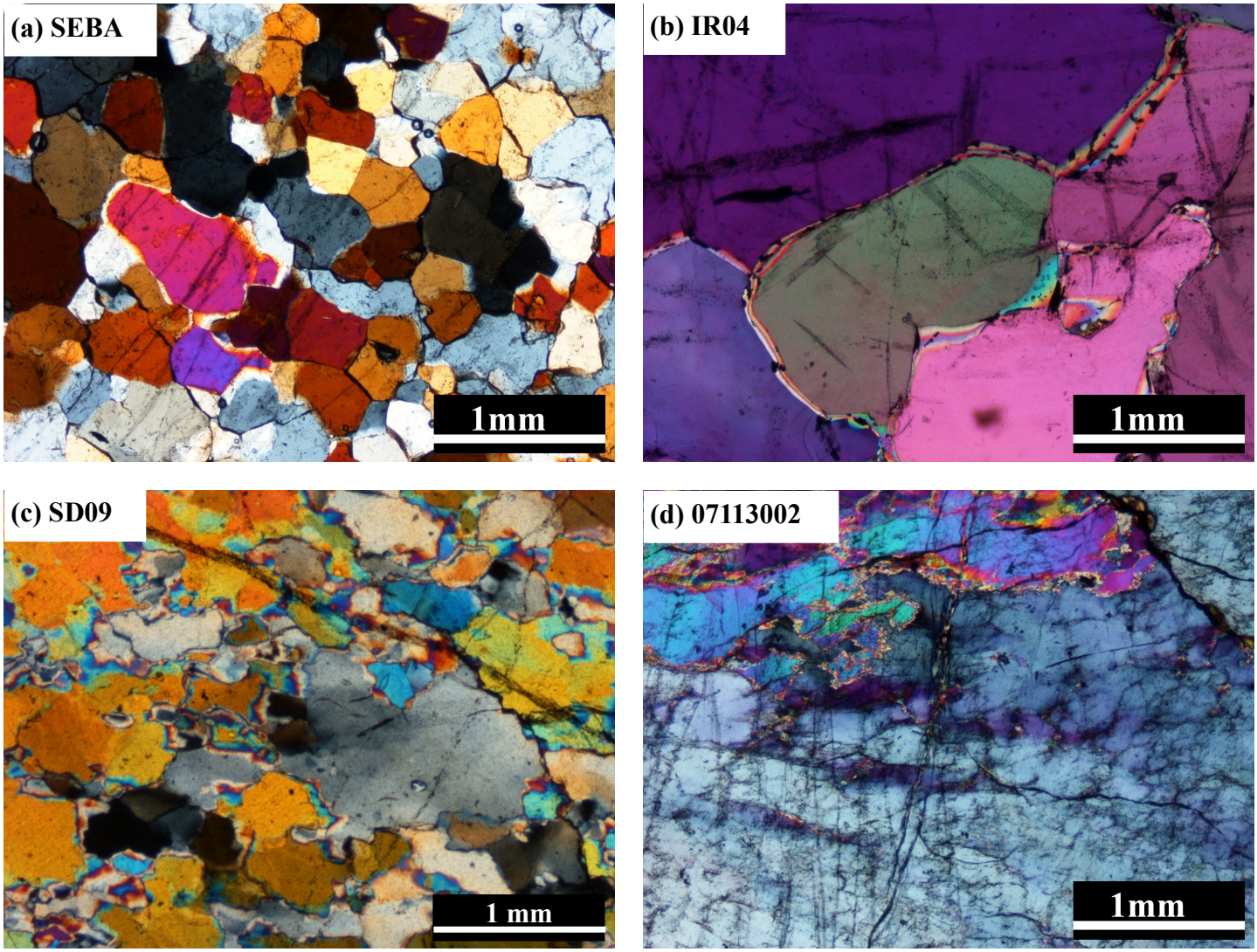

Fig.3. Typical quartz fabrics of (a-b) coarse grained P-type veins; (c) DI-type vein; (d) DD-type vein.

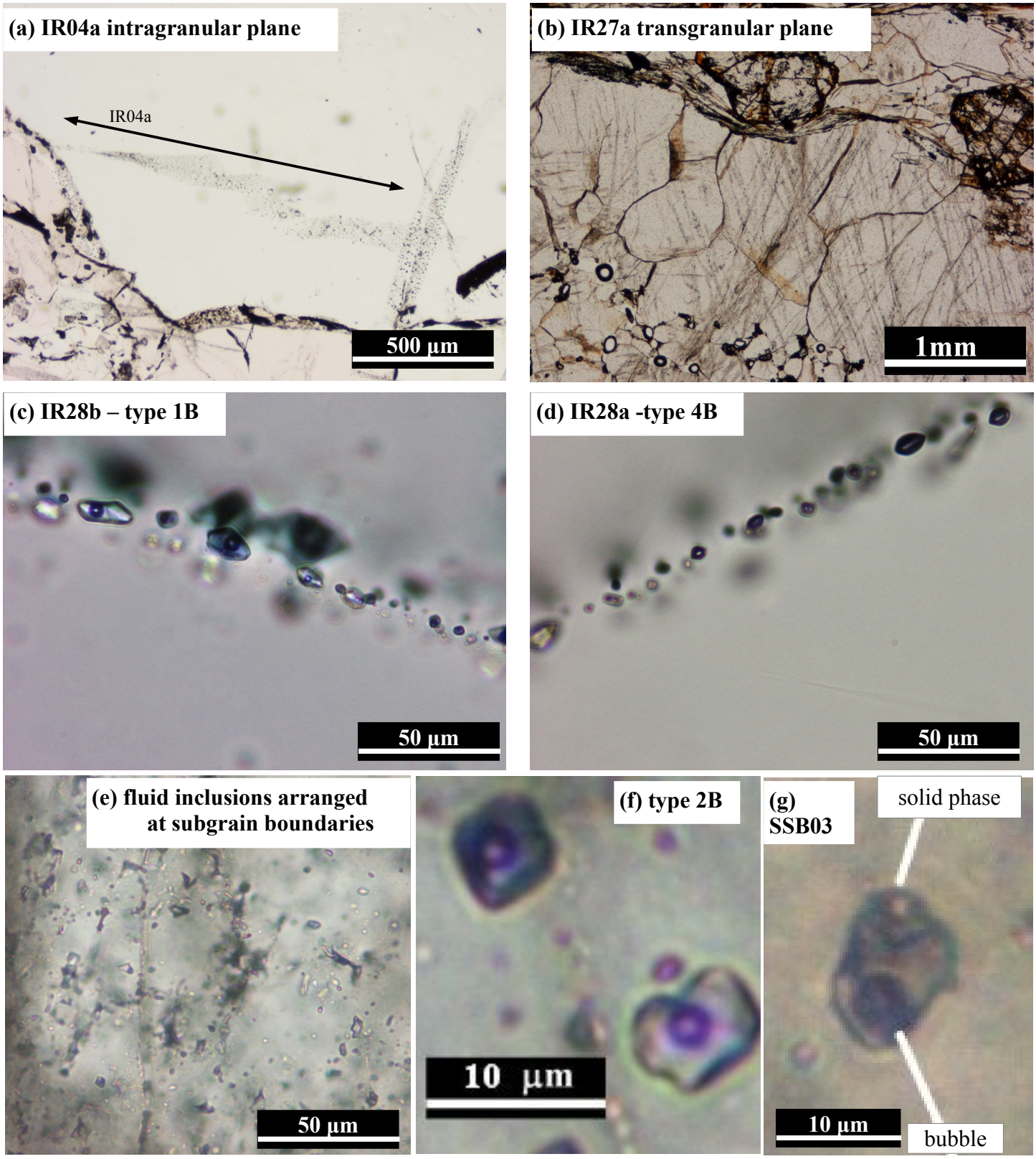

Fig.4. Typical occurrences of fluid inclusions. (a) Fluid inclusions arranged along intragranular planes (IR04a). (b) Type 2B fluid inclusions which are characterized by high-saline aqueous fluid, and are generally arranged along transgranular planes (IR27a). (c) Typical fluid inclusions of type 1B which are characterized by diluted aqueous fluid and are generally arranged at transgranular planes. (d) Dark colored type 4B fluid inclusions which are characterize by anhydrous composition and are generally arranged at transgranular planes. (e) Fluid inclusions arranged at subgrain boundaries observed in 10AS18. (f) Close-up photo of inclusions of IR27a composed of aqueous fluid and CH_4-N_2 gas. (g) A type 3 inclusion of SSB03 containing solid, bubble and liquid phases.

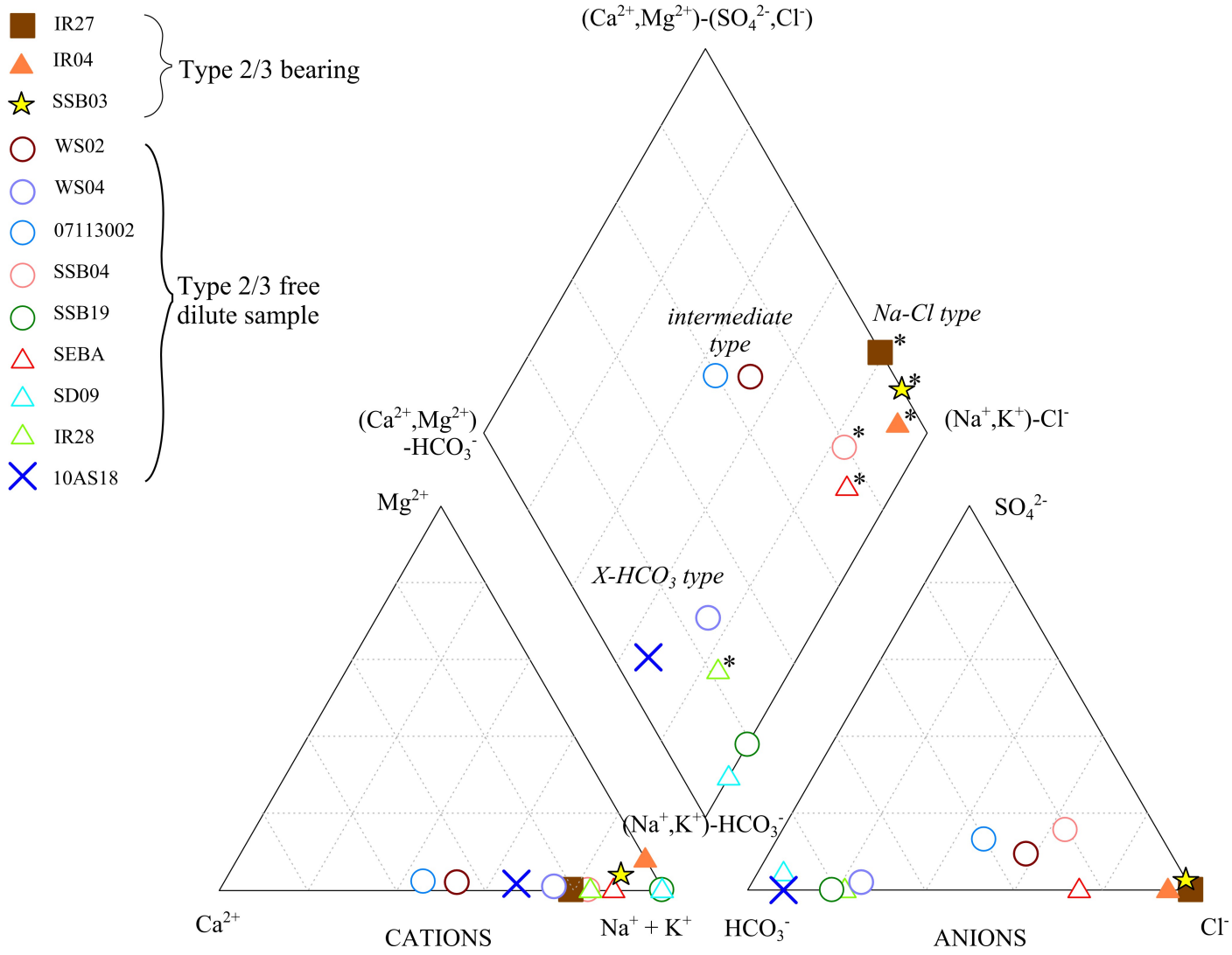

Fig.5. Hydrochemical characteristics of the crush-leached fluids plotted in a Piper's diagram. Ternary diagrams in the left-bottom and right-bottom show relative compositions of cations [Mg^{2+}-Ca^{2+}-(Na, K)$^{+}$] and anions [SO_4^{2-}-HCO_3^{-}-Cl^{-}], respectively. Asterisks (*) indicate data obtained from P-type quartz veins. The rhomboid-cation-anion plot shows that Na and Cl are primary components in P-type quartz veins.

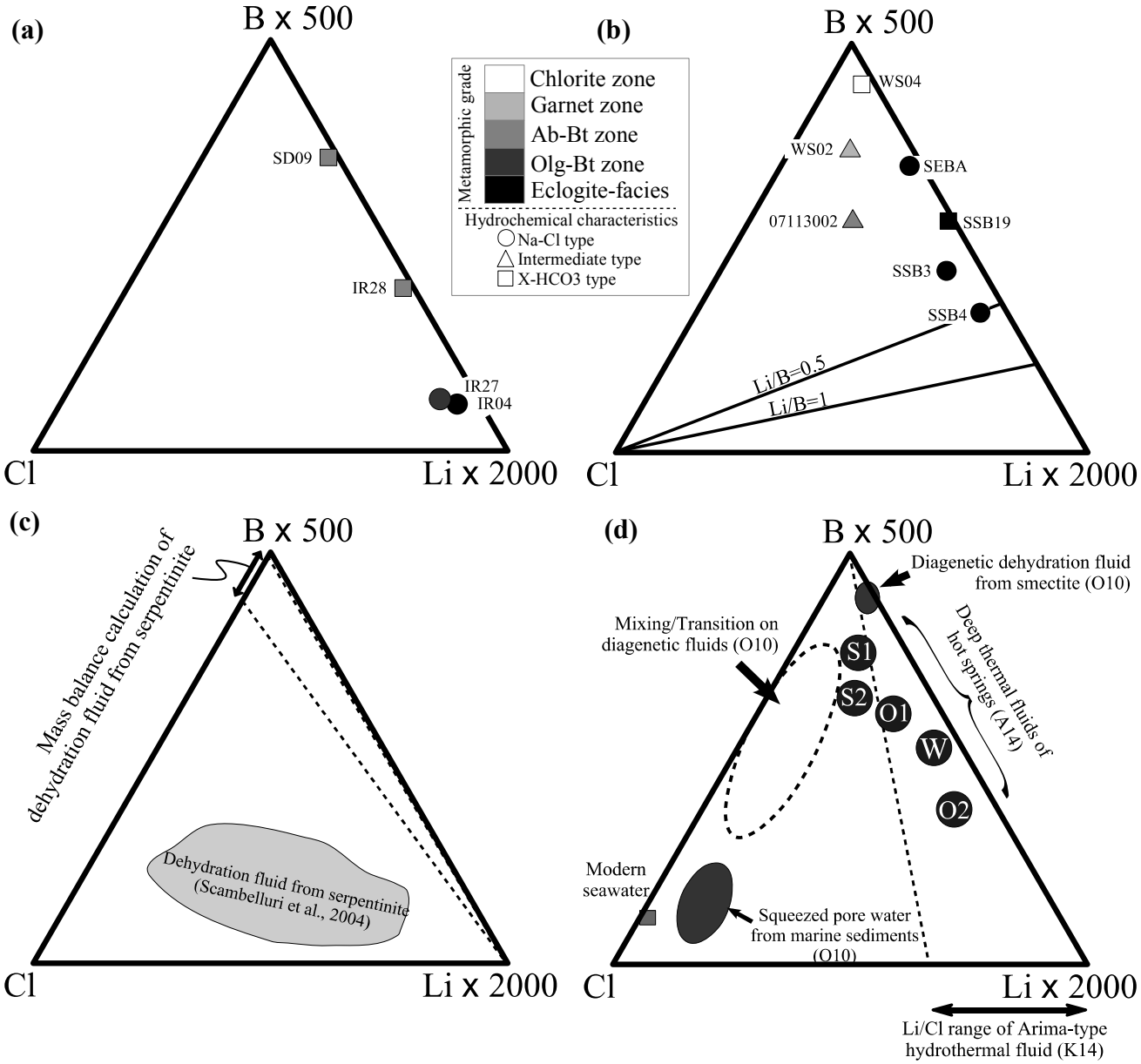

Fig.6. B-Li-Cl ternary diagram plotted after Ohsawa et al. (2010). (a-b) Compositions of crush-leached fluid concerning the lithotype of host rock, for (a) metasediment rock and (b) meta-mafic rock hosted veins, respectively. Symbols of circle, square and triangle represent Na-Cl, X-HCO_3 and intermediate type hydrochemical characteristics, respectively. The filled grey-scale represents the metamorphic grade of the host rocks, i.e. the darker the color, the higher the metamorphic grade. (c) B-Li-Cl compositions of fluid inclusions contained in olivine and calculated B/Cl ratio of the dehydrated fluid and mass balance calculation results obtained from serpentinite dehydration (Scambelluri et al., 2004). (d) Compositions of hydrothermal fluids obtained from hot springs in the fore-arc region in SW Japan (Ohsawa et al., 2010; Amita et al., 2014) and Li/Cl range of Arima-type hydrothermal fluids (K14: Kazahaya et al., 2014). O10 and A14 represent Ohsawa et al. (2010) and Amita et al. (2014) respectively. Among the data points of Amita et al. (2014), S1 and S2 are obtained from the Shikoku area, W is from the Wakayama area, and O1 and O2 are from the Oita area.

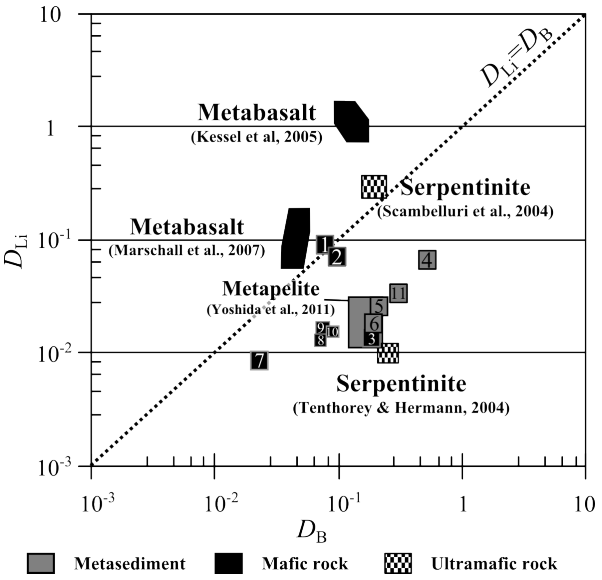

	rock type	method
Scambelluri et al. (2004)	serpentinite	mass balance calculation based on the mineral abundance of natural samples
Tenthorey and Hermann (2004)	serpentinite	experimentally measured
Kessel et al. (2005)	K_2O-free MORB	experimentally measured
Marschall et al. (2007)	K_2O-added MORB	calculation based on pseudosection modeling of the subducting MORB
Yoshida et al. (2011)	pelite	calculation based on pseudosection modeling of the subducting pelite
this study	mafic and sedimentary rocks	calculation based on the measured mineral abundances of the sample

Fig.7. Partition coefficient data of B and Li between whole rock and aqueous fluid (concentration in rock/ concentration in aqueous fluid) from this study and previous ones. Methods used in previous studies are also summarized at right. Numbered boxes are samples from this study. Numbers refer: (1) WS04; (2) WS02; (3) 07113002; (4) SD09; (5) IR28; (6) IR27; (7) SSB03; (8) SSB04; (9) SEBA; (10) SSB19; (11) IR04.

Table 1. Estimated mineral abundances in host metamorphic rocks of the studied quartz veins.

Sample	grade	Rock type	Ttn	Rt	Grt	Ep	Cpx	Amp	Chl	Bt	Ph	Pg	Pl	Qz	Other minerals	Method
WS04	Chl	mafic	12.2			25.0		17.4	29.5		8.8		6.8	0.1	Cal, Ccp	**
WS02	Grt	mafic	2.3			24.1		21.2	18.8		9.6		14.6†	0.1	Cal, Ap	**
07113002	Ab-Bt	mafic	5.9			13.3		11.7			22.1		40.4	2.5	Cal, Ap, Ccp	**
SD09	Ab-Bt	pelitic	2nd	1.0	1.6				9.8		66.4		7†	13	Cal, Ap	**
IR28	Ab-Bt	pelitic	2nd		2.3			13.7	3.6		28.1		0.4	52.0		**
IR27	Olig-Bt	pelitic	0.7	<0.1	0.9	3.2		6.8	1.5		24.3	0.1	20.6	40.4	Hem	*
SSB03	ECL	mafic	2nd			32.6		49.3	1.8		0.7		13.6		Cal	***
SSB04	ECL	mafic		1.9	22	12.4		51.8	2		8.6		0.5†	0.4	Hem	**
SEBA	ECL	mafic	2.0		10.9	4.5	1.6	10.5	1.6	6.0	7.4		21.6	15.2	abundant Cal, Hem	**
SSB19	ECL	mafic	2nd	0.7	7.8	10.4	1.7	50.7	1.4		10.8		10.6	3.8	Cal, Hem	**
IR04	ECL	sedimentary	2nd	1.0	7.7			41.8	3.8		43.0		2.7		Apt	**

Estimation methods are *: semi-quantitative analysis by EDS; **: X-ray chemical mapping; ***: optical microscopy. † occurring as large porphyroblasts and are conisidered to be retrograde origin. 2nd: Titanite observed at the rim of rutile, and observed scarce amount.

Table 2. Summary of textural and chemical characteristics of fluid inclusions observed in the studied samples. Quartz fabric characteristics are also included.

Sample	Mineral zone	Host rock type	Qz-Fabric	FI-group	FI-type	Textural appearance	Size (μm)	Abundance	*n*/ phases	T_m(ice) (ºC)	T_m Average	T_h(total) (ºC)	T_h Average	Total salinity (mass%$_{NaCleq}$)	Chemical species
WS04	Chl	mafic	DD	WS04a	1C	Subgrain boundary	<5	+++	2/L-V	-0.1 to -3.3	-1.8	120 to 255	194	0.2 to 5.4	Aq
WS02	Grt	mafic	DD	WS02a	1B	Transgr. FIP	5 to 10	+++	2/L-V	-0.1 to -4.1	-1.6	160 to 280	176	0.2 to 9.2	Aq-N_2
07113002	Ab-Bt	mafic	DD	07113002a	1B	Transgr. FIP	<5	++	2/L-V	-0.4 to -3.6	-2.0	140 to 245	170	0.7 to 5.9	Aq
SD09	Ab-Bt	pelitic	DI	SD09a	4A	Intragr. FIP	~5	+	1/V	——		——		-	CO_2-N_2-CH_4
				SD09b	1B	Transgr. FIP	3 to 15	++	2/L-V	-0.2 to -1.6	-0.7	170 to 275	220	0.4 to 2.7	Aq-CH_4-N_2
IR28	Ab-Bt	pelitic	P	IR28a	4B	Transgr. FIP	5 to 40	++	1/V	——		——		-	N_2-CH_4
				IR28b	1B	Transgr. FIP	1 to 20	++	2/L-V	-0.5 to -1.3	-0.7	198 to 241	213	0.9 to 2.2	Aq-N_2-CH_4
IR27	Olg-Bt	pelitic	P	IR27a	2B	Transgr. FIP	1 to 15	+++	2/L-V	-3.4 to -7.1	-5.1	154 to 276	202	5.7 to 10.5	Aq-N_2-CH_4
				IR27b	-	Intragr. FIP	<3	+	2/L-V	*		*		*	unidentified
SSB03	ECL	mafic	P	SSB03a	2B	Transgr. FIP	~20	+++	2/L-V	-3.0 to -18.0	-8.6	210 to 350	249	1.7 to 21.0	Aq-N_2-CH_4
				SSB03b	4B	Transgr. FIP	5 to 10	+	1/V	——		——		-	N_2
				SSB03c	3	Isolated	~10	+	3/L-V-S	above halite saturation		312		above halite saturation	Aq
SSB04	ECL	mafic	P	SSB04a	1B	Transgr. FIP	5 to 15	++	2/L-V	-1.1 to -1.3	-1.2	207 to 275	241	1.9 to 2.2	Aq-N_2-CH_4
				SSB04b	1B	Transgr. FIP	5 to 15	+++	2/L-V	-0.1 to -0.3	-0.2	215 to 259	241	0.2 to 0.5	Aq-N_2
				SSB04c	4A	Intragr. FIP	5 to 15	+	1/V	——		——		-	CO_2-N_2-CH_4
SEBA	ECL	mafic	P	SEBAa	1B	Transgr. FIP	5 to 20	++	2/L-V	-0.4 to -2.1	-1.2	150 to 270	226	0.7 to 3.6	Aq-N_2-CH_4
SSB19	ECL	mafic	DI	SSB19a	1B	Transgr. FIP	5 to 15	+++	2/L-V	0.0 to -0.3	-0.2	166 to 257	219	0.0 to 0.5	Aq-N_2
IR04	ECL	sedimentary	P	IR04a	2A	Intragr. FIP	1 to 15†	+	2/L-V	-4.4 to -5.6	-4.9	190 to 269	228	7.0 to 8.7	Aq-CH_4
				IR04b	4A	Intragr. FIP	5 to 20	++	2/L-V	——		——		-	CO_2-N_2-CH_4-H_2
				IR04c	2B	Transgr. FIP	1 to 10	+++	2/L-V	-5.7 to -6.2	-6.0	218 to 255	230	8.7 to 9.5	Aq-N_2-CH_4
10AS18	LS vein /Chl	pelitic	DD	10AS18a	1C	Subgrain boundary	<20	+++	2/L-V	-0.6 to -1.4	-1.0	99 to 210	137	1.1 to 2.4	Aq

Abundance of fluid inclusions are; +++: abundant; ++: common; +: rare. Aq: aqueous fluid; *: not determined due to its small size; LS means later stage (for details, see text); †except for annular shaped ones (~30 μm).

Table 3. Chemical compositions of extracted fluids obtained by the crush-leach method.

Sample	Mineral zone	Host rock type	Qz fabric	Hydrochemical characteristics	Na (mg/L)	NH_4 (mg/L)	K (mg/L)	Mg (mg/L)	Ca (mg/L)	F (mg/L)	Cl (mg/L)	SO_4 (mg/L)	HCO_3 (mg/L)	Li (μg/L)	B (μg/L)	Li/B	(B+Li)/Cl ($\times 10^{-3}$)
SSB04	ECL	mafic	P	Na-Cl	***0.8***	**0.3**	0.2	0	0.1	0.1	***1.7***	-0.04	**0.99**	8.59	19.5	0.44	16.5
SEBA	ECL	mafic	P	Na-Cl	***0.9***	0.4	**0.4**	0	0.2	0	***0.9***	0.3	**0.5**	4.3	44	0.10	53.7
SSB3	ECL	mafic	P	Na-Cl	***3.7***	0.3	**0.6**	0.1	0.3	0	***5.3***	**0.2**	0	16	59	0.27	14.2
IR04	ECL	sedimentary	P	Na-Cl	***2.1***	0.1	**0.2**	0.1	0	0	***4.3***	-0.05	**0.44**	36.89	18.5	1.99	12.9
IR27	Olg-Bt	pelitic	P	Na-Cl	***4.3***	0.1	**0.9**	0	1.1	0	***12.2***	0	0	63.89	37.5	1.70	8.3
IR28	Ab-Bt	pelitic	P	K-HCO3	**0.3**	0	***0.5***	0	0.1	0	**0.4**	0	***2.44***	5.29	14.5	0.36	49.5
SSB19	ECL	mafic	DI	K-HCO3	**0.2**	0	***0.7***	0.0	0.0	0	**0.2**	-0.01	***1.47***	2.89	15.5	0.19	92.0
SD9	Ab-Bt	pelitic	DI	K-HCO3	**0.2**	0.2	***0.3***	0	0	0	0.1	0.1	***2.6***	0.7	8.2	0.09	89.0
07113002	Ab-Bt	mafic	DD	intermediate	**4.43**	0.54	0.49	0.12	***4.83***	0.12	**7.94**	3.03	***11.73***	4	42	0.10	5.8
WS02	Grt	mafic	DD	intermediate	***4.45***	0.47	0.51	0.09	**3.53**	0.11	***8.46***	1.85	**8.13**	4	94	0.04	11.6
WS04	Chl	mafic	DD	Na-HCO3	***6.34***	0.33	0.03	0.04	**1.79**	0.13	**3.34**	0.37	***16.96***	4	200	0.02	61.1
10AS18	p-C	pelitic	DD	Na-HCO3	***5.78***	0.34	0.37	0.08	**2.53**	0	**0.89**	0	***17.69***	-	-	-	-

Host rock type: b/p/s are basic/pelitic/sedimentary, respectively and Chl/Grt/Ab-Bt/Olg-Bt/ECL are chlorite/garnet/albite-biotite/oligoclase-biotite zones and eclogite, respectively. ***Bold and italic*** and **bold** lettering show the highest and second highest values, respectively, among cations and anions.

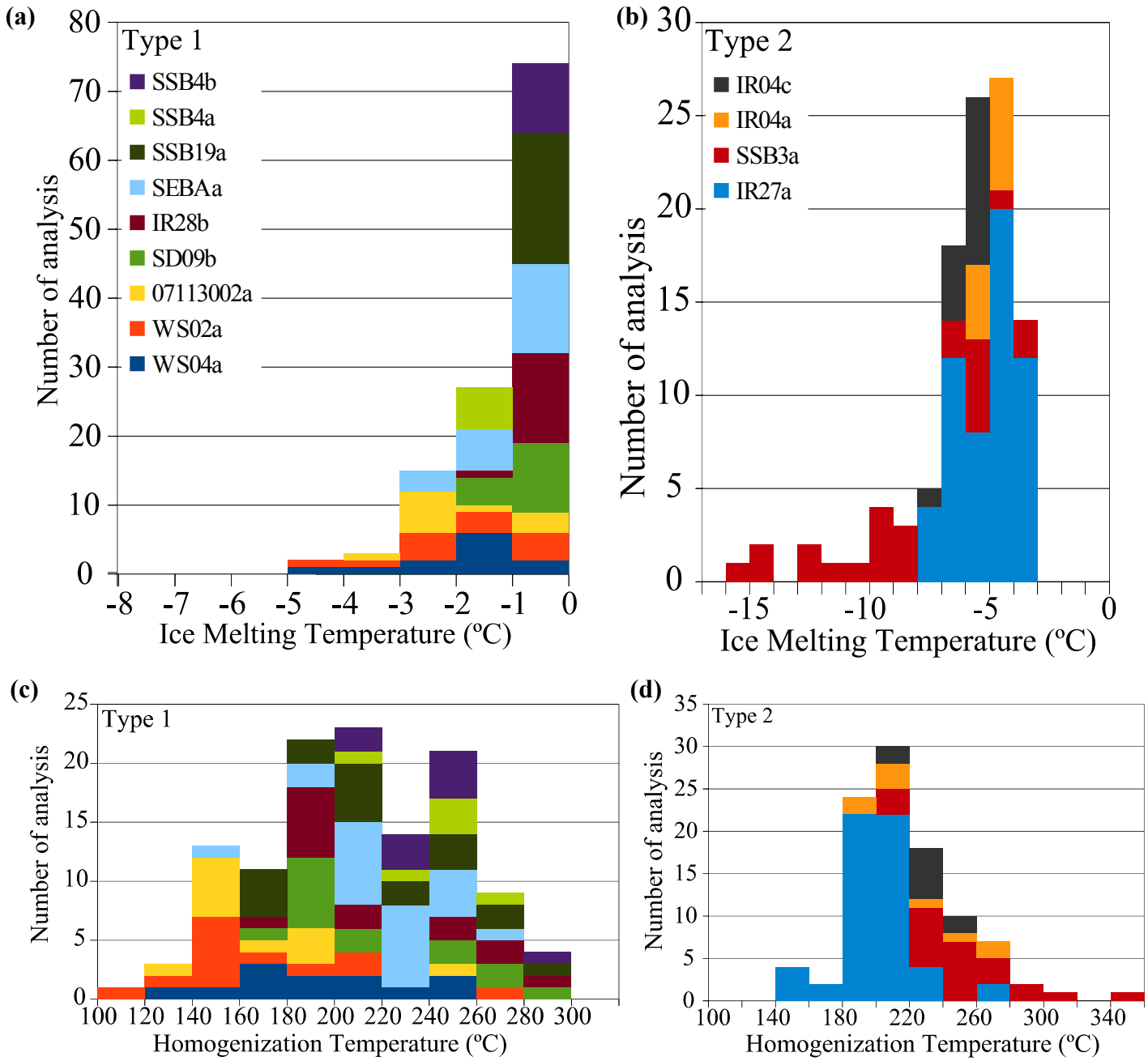

Fig.S1. Histograms of the results of microthermometry. (a) and (b) are ice melting temperature of type 1 and 2, respectively. (c) and (d) are homogenization temperature of type 1 and 2, respectively.

Table S1. Representative chemical composition of amphiboles

Sample	WS04	WS02	07113002	SD09	IR28	IR27	SSB03	SSB04	SEBA	SSB19	IR04
Mineral	Amp	Amp	Amp	-	Amp	Amp	Amp	Amp	Amp	Amp	Amp
SiO_2	55.37	53.14	54.21	-	45.49	44.56	48.36	48.62	42.43	47.59	45.85
TiO_2	0.00	0.21	0.14	-	0.40	0.34	0.45	0.47	0.32	0.53	0.48
Al_2O_3	1.26	4.16	1.70	-	14.52	15.25	10.52	10.30	14.96	12.21	14.51
Cr_2O_3	0.00	0.09	0.00	-	0.06	0.00	0.02	0.02	0.00	0.00	0.01
FeO*	14.65	10.62	13.59	-	12.62	13.52	13.76	14.76	19.13	13.94	13.65
MnO	0.32	0.20	0.40	-	0.08	0.07	0.22	0.08	0.10	0.06	0.17
MgO	14.42	16.01	15.22	-	11.69	10.37	11.61	12.10	7.48	11.40	11.17
CaO	11.76	10.13	10.19	-	9.63	10.23	8.11	7.42	10.14	8.57	10.32
Na_2O	0.78	2.15	1.67	-	2.62	2.53	3.85	3.67	3.06	3.92	2.24
K_2O	0.10	0.12	0.09	-	0.44	0.46	0.45	0.35	0.78	0.52	0.37
BaO	0.02	0.00	0.06	-	0.03	0.04	0.00	0.14	0.00	0.01	0.02
F	0.00	0.00	0.00	-	0.00	0.00	0.00	0.00	0.00	0.00	0.00
-O=F	0.00	0.00	0.00	-	0.00	0.00	0.00	0.00	0.00	0.00	0.00
Cl	0.01	0.00	0.00	-	0.00	0.01	0.00	0.00	0.00	0.00	0.00
-O=Cl	0.00	0.00	0.00	-	0.00	0.00	0.00	0.00	0.00	0.00	0.00
total	98.64	96.82	97.20	-	97.55	97.33	97.35	97.75	98.40	98.72	98.78
Number of ions on the basis of 23 O				-							
Si	7.92	7.58	7.77	-	6.50	6.46	6.98	6.91	6.30	6.79	6.51
Ti	0.00	0.02	0.01	-	0.04	0.04	0.05	0.05	0.04	0.06	0.05
Al	0.21	0.70	0.29	-	2.45	2.61	1.79	1.72	2.62	2.05	2.43
Cr	0.00	0.01	0.00	-	0.01	0.00	0.00	0.00	0.00	0.00	0.00
Fe^{3+}	0.11	0.38	0.53	-	0.71	0.41	0.49	1.03	0.46	-6.64	0.62
Fe^{2+}	1.65	0.88	1.10	-	0.80	1.23	1.17	0.73	1.92	7.86	1.00
Mn	0.04	0.02	0.05	-	0.01	0.01	0.03	0.01	0.01	0.01	0.02
Mg	3.07	3.40	3.25	-	2.49	2.24	2.50	2.56	1.66	2.43	2.37
Ca	1.80	1.55	1.57	-	1.47	1.59	1.25	1.13	1.61	1.31	1.57
Na	0.21	0.59	0.46	-	0.73	0.71	1.08	1.01	0.88	1.08	0.62
K	0.02	0.02	0.02	-	0.08	0.09	0.08	0.06	0.15	0.10	0.07
Ba	0.00	0.00	0.00	-	0.00	0.00	0.00	0.01	0.00	0.00	0.00
F	0.00	0.00	0.00	-	0.00	0.00	0.00	0.00	0.00	0.00	0.00
Cl	0.00	0.00	0.00	-	0.00	0.00	0.00	0.00	0.00	0.00	0.00

Table S2. Representative chemical composition of micas

Sample	WS04	WS02	07113002	SD09	IR28	IR27	SSB03	SSB04	SEBA		SSB19	IR04
Mineral	Ph	Ph	Ph	Ph	Ph	Ph	Ph	Ph	Ph	Bt	Ph	Ph
SiO_2	51.09	49.82	48.30	48.19	48.60	48.95	49.44	50.07	50.09	37.38	50.28	49.35
TiO_2	0.07	0.27	0.22	0.21	0.51	0.55	0.47	0.60	0.34	1.29	0.43	0.73
Al_2O_3	22.96	26.58	23.95	29.73	32.35	30.98	26.82	26.35	27.61	16.05	27.75	32.11
Cr_2O_3	0.09	0.07	0.00	0.03	0.01	0.03	0.20	0.03	0.00	0.03	0.00	0.05
FeO*	5.08	3.44	7.22	3.02	1.39	1.66	4.00	3.70	2.46	18.96	2.93	1.76
MnO	0.03	0.00	0.10	0.00	0.02	0.00	0.00	0.00	0.00	0.08	0.00	0.09
MgO	4.31	3.42	3.01	2.47	1.84	2.10	2.91	3.00	3.03	10.60	2.97	2.12
CaO	0.09	0.01	0.01	0.00	0.00	0.02	0.00	0.00	0.00	0.00	0.04	0.03
Na_2O	0.07	0.52	0.12	0.65	1.27	1.47	0.74	0.63	0.71	0.12	0.66	0.89
K_2O	10.70	10.62	10.92	9.88	9.01	8.92	10.13	10.06	10.24	9.45	10.12	8.87
BaO	0.04	0.14	0.19	0.03	0.39	0.28	0.21	0.05	0.12	0.08	0.10	0.25
F	0.00	0.02	0.00	0.04	0.02	0.00	0.00	0.00	0.01	0.00	0.00	0.00
-O=F	0.00	0.01	0.00	0.02	0.01	0.00	0.00	0.00	0.00	0.00	0.00	0.00
Cl	0.00	0.00	0.01	0.00	0.01	0.00	0.00	0.00	0.00	0.01	0.00	0.00
-O=Cl	0.00	0.00	0.00	0.00	0.00	0.00	0.00	0.00	0.00	0.00	0.00	0.00
Total	94.49	94.75	93.85	94.17	94.97	94.70	94.72	94.43	94.47	93.95	95.18	96.00
Number of the ions on the basis of 11 O												
Si	3.50	3.38	3.44	3.26	3.22	3.26	3.36	3.39	3.37	2.88	3.37	3.23
Ti	0.00	0.01	0.01	0.01	0.03	0.03	0.02	0.03	0.02	0.07	0.02	0.04
Al	1.85	2.12	2.01	2.37	2.53	2.43	2.15	2.11	2.19	1.46	2.19	2.48
Cr	0.01	0.00	0.00	0.00	0.00	0.00	0.01	0.00	0.00	0.00	0.00	0.00
Fe^{3+}	0.15	0.13	0.11	0.10	0.03	0.05	0.14	0.10	0.06	0.00	0.08	0.05
Fe^{2+}	0.14	0.07	0.69	0.07	0.04	0.04	0.09	0.11	0.08	1.22	0.09	0.05
Mn	0.00	0.00	0.01	0.00	0.00	0.00	0.00	0.00	0.00	0.01	0.00	0.01
Mg	0.44	0.34	0.32	0.25	0.18	0.21	0.29	0.30	0.30	1.22	0.30	0.21
Ca	0.01	0.00	0.00	0.00	0.00	0.00	0.00	0.00	0.00	0.00	0.00	0.00
Na	0.01	0.07	0.02	0.08	0.16	0.19	0.10	0.08	0.09	0.02	0.09	0.11
K	0.93	0.92	0.99	0.85	0.76	0.76	0.88	0.87	0.88	0.93	0.86	0.74
Ba	0.00	0.00	0.01	0.00	0.01	0.01	0.01	0.00	0.00	0.00	0.00	0.01
F	0.00	0.00	0.00	0.01	0.00	0.00	0.00	0.00	0.00	0.00	0.00	0.00
Cl	0.00	0.00	0.00	0.00	0.00	0.00	0.00	0.00	0.00	0.00	0.00	0.00
Total	7.05	7.05	7.60	7.02	6.97	6.98	7.04	7.00	7.00	7.80	6.99	6.92

Table S3. Representative chemical composition of apatites

Sample	WS02	07113002	SD09	IR04
Mineral	Ap	Ap	Ap	Ap
SiO_2	0.04	0.02	0.05	0.00
TiO_2	0.09	0.03	0.24	0.00
Al_2O_3	0.00	0.00	0.00	0.01
Cr_2O_3	0.02	0.04	0.03	0.00
FeO*	0.08	0.13	0.05	0.15
MnO	0.05	0.04	0.00	0.02
MgO	0.01	0.03	0.00	0.05
CaO	55.16	55.28	55.29	54.62
Na_2O	0.00	0.00	0.00	0.00
K_2O	0.00	0.01	0.01	0.00
P_2O_5	45.33	44.08	45.93	42.65
BaO	0.00	0.00	0.00	0.00
F	2.95	2.89	3.72	2.39
-O=F	1.24	1.22	1.57	1.00
Cl	0.00	0.00	0.00	0.02
-O=Cl	0.00	0.00	0.00	0.00
total	102.49	101.33	103.75	98.88
Number of cations on the basis of 26 (O, OH, F, Cl)				
Si	0.01	0.00	0.01	0.00
Ti	0.01	0.00	0.03	0.00
Al	0.00	0.00	0.00	0.00
Cr	0.00	0.01	0.00	0.00
Fe^{2+}	0.01	0.02	0.01	0.02
Mn	0.01	0.01	0.00	0.00
Mg	0.00	0.01	0.00	0.01
Ca	9.33	9.51	9.13	9.72
Na	0.00	0.00	0.00	0.00
K	0.00	0.00	0.00	0.00
P	6.06	5.99	5.99	6.00
Ba	0.00	0.00	0.00	0.00
F	1.47	1.47	1.81	1.25
Cl	0.00	0.00	0.00	0.01